The relationships between regional Quaternary uplift, deformation across active normal faults and historical seismicity in the upper plate of subduction zones: The Capo D'Orlando Fault, NE Sicily.

M. Meschis[1*], G.P. Roberts[1], J. Robertson[1] and R.M. Briant[2].

[1]Department of Earth and Planetary Sciences, Birkbeck, University of London, WC1E 7HX, UK.

[2]Department of Geography, Environment and Development Studies, Birkbeck, University of London, WC1E 7HX, UK

Abstract

In order to investigate deformation within the upper plate of the Calabrian subduction zone we have mapped and modelled a sequence of Late Quaternary palaeoshorelines tectonically-deformed by the Capo D'Orlando normal fault, NE Sicily, which forms part of the actively deforming Calabrian Arc. In addition to the 1908 Messina Strait earthquake (Mw 7.1), this region has experienced damaging earthquakes, possibly on the Capo D'Orlando Fault, however, it is not considered by some to be a potential seismogenic source. Uplifted Quaternary palaeoshorelines are preserved on the hangingwall of the Capo D'Orlando Fault, indicating that hangingwall subsidence is counteracted by regional uplift, likely because of deformation associated with subduction/collision. We attempt to constrain the relationship between regional uplift, crustal extensional processes and historical seismicity, and we quantify both the normal and regional deformation signals. We report uplift variations along the strike of the fault and use a synchronous correlation technique to assign ages to palaeoshorelines, facilitating calculation of uplift rates and the fault throw-rate. Uplift rates in the hangingwall increase from 0.4 mm/yr in the centre of the fault to 0.89 mm/yr beyond its SW fault tip, suggesting 0.5 mm/yr of fault related subsidence, which implies a throw-rate of 0.63 ± 0.02 mm/yr, and significant seismic hazard.

Overall, we emphasise that upper plate extension and related vertical motions complicate the process of deriving information on the subduction/collision process, such as coupling and slip distribution on the subduction interface, parameters that are commonly inferred for other subduction zones without considering upper plate deformation.

*Corresponding author.

E-mail address: marco.meschis.14@ucl.ac.uk (M. Meschis)

1. Introduction

Data on coastal uplift in the upper plate of subduction zone are commonly used to infer the slip distributions and gain insight into the processes of coupling along the subduction interface and mantle upwelling [*McCloskey et al.*, 2005; *Meltzner et al.*, 2006; *Nalbant et al.*, 2013; *Nic Bhloscaidh et al.*, 2015; *D'Agostino et al.*, 2001; *Faure Walker et al.*, 2012; *Faccenna et al.*, 2014]. This paper emphasises that there is a growing body of evidence that the upper plates of subduction zones can also be deformed by active normal faults. This evidence is widespread for example from central Greece and Crete [*Armijo et al.*, 1992; *Papanikolaou et al.*, 2006; *Gallen et al.*, 2014], south America [*Saillard et al.*, 2011; *Binnie et al.*, 2016], New Zealand [*Nicol and Beavan*, 2003], Japan [*Hasegawa et al.*, 2000] and southern Italy [*Monaco and Tortorici*, 2000; *Jacques et al.*, 2001; *Spampinato et al.*, 2012; *Roberts et al.*, 2013]. Deformation related to normal faulting must be removed if the observed coastal uplift is to be used to constrain both the slip-distribution on the subduction interface and mantle dynamics-related topography.

Long-term crustal extension processes occurring in Calabria and NE Sicily have been accommodated by active normal faults that have been deforming palaeoshorelines through the Late

Quaternary [*Monaco and Tortorici*, 2000; *Jacques et al.*, 2001; *Catalano and De Guidi*, 2003; *Giunta et al.*, 2012; *Roberts et al.*, 2013]. The locations of historical damaging earthquakes from Italian catalogues [*Guidoboni et al.*, 2007; *Stucchi et al.*, 2013] lie close to these mapped normal faults [*Monaco and Tortorici*, 2000; *Galli et al.*, 2008; *Roberts et al.*, 2013] . Potential seismogenic sources have been collated within the Database of Individual Seismogenic Source (DISS) [*Basili et al.*, 2008], providing a base from which to define the geography of seismic hazard in Italy. However, we ask whether the locations of all active normal faults that can be considered to be candidate seismogenic sources are known. For example, even though two well-documented medium-magnitude historical seismic events have been reported [*Guidoboni et al.*, 2007] around the Capo D'Orlando area, in NE Sicily, only a few studies [*Scicchitano et al.*, 2011; *Giunta et al.*, 2012] have attempted to identify plausible potential seismogenic sources, such as the Capo D'Orlando Fault. These authors recognised that Quaternary palaeoshorelines are tilted and hence deformed by the Capo D'Orlando Fault, suggesting the fault is active. However, the results are considered equivocal by some, for example because no active faults are reported in this location within the DISS [*Basili et al.*, 2008] . In this study, we investigate whether the Capo D'Orlando Fault reported by *Scicchitano et al.* [2011] and *Giunta et al.*, [2012] should be added to the DISS.

A quantitative understanding of Late Quaternary upper-crustal vertical movements such as tectonic uplift and/or subsidence and their associated slip-rates on active normal faults within a plate boundary region is fundamental to long-term seismic hazard assessment [*Roberts et al.*, 2013]. We take into account the notion that any evidence of fault movement since the Middle/Late Pleistocene has been accepted by some as the definition of an "active fault" [*Yeats*, 2012; *Chapman et al.*, 2014]. Therefore, we study the long-term deformation since the Middle Pleistocene by investigating sequences of deformed palaeoshorelines, which can be used to (i) help differentiate between transitory strain-rates associated with temporal earthquake clustering, and (ii) judge how long-term strain-rates measured over many seismic cycles relate to those measured over shorter timescales [*Yeats and Prentice*, 1996; *Ward*, 1998; *Friedrich et al.*, 2003; *Papanikolaou et al.*, 2005; *Faure Walker et al.*, 2010; *Roberts et al.*, 2013].

The approach that we have taken is to examine differential uplift across the candidate active fault in question [*Massonnet et al.*, 1993; *Massonnet and Feigl*, 1995; *Armijo et al.*, 1996; *Roberts et*

al., 2009, 2013; *Walters et al.*, 2009; *Papanikolaou et al.*, 2010]. In particular, we focus our attention on the 15 km onshore section of the NE–SW oriented Capo D'Orlando Fault [*Scicchitano et al.*, 2011; *Giunta et al.*, 2012]. We conduct new mapping alongside a review of ages for previously-mapped palaeoshorelines outcropping on the hangingwall of the Capo D'Orlando Fault. The age review is conducted by attempting to correlate palaeoshorelines that are unevenly spaced in elevation with glacio-eustatic sea-level highstands that are unevenly spaced in time through iteration of the uplift rate history [*Roberts et al.*, 2009, 2013]. This work (i) quantifies uplift rates values, (ii) investigates along-strike variation in uplift rate, which if correlated with the fault offset and fault-tip locations, will confirm Quaternary activity on the fault, (iii) investigates rates of tilting for palaeoshorelines along the strike of the fault to define displacement gradients, and (iv) estimates the associated slip-rate through correlation between offset palaeoshorelines preserved in the hangingwall and footwall, which has fundamental tectonic and seismic hazard implications [*Cowie et al.*, 2012]. We investigate the above by mapping the inner edges of marine terraces (palaeoshorelines) both through detailed topographic surveying using a 10-m resolution Digital Elevation Model (DEM) [*Tarquini et al.*, 2007, 2012] and fieldwork, seeking to confirm the reliability of the mapping by *Giunta et al.* [2012]. We then correlate our mapped inner edge elevations with glacio-eustatic sea-level highstands since the Middle Pleistocene, by iterating the uplift-rate. We assess the robustness of our correlations between multiple mapped palaeoshorelines and multiple sea-level highstands through linear regression analysis. Finally, we discuss our results in terms of local and regional tectonic implications and seismic hazard assessment within the Ionian subduction zone and the associated Plio-Pleistocene regional extensional processes, which are accommodated by several upper crustal active normal faults potentially producing damaging earthquakes.

2. Background

2.1. Geological background

The study area lies in the southernmost part of the Calabrian Arc, which forms the link between the NW–SE oriented southern Apennines thrust belt in mainland Italy and the E-W oriented Maghrebide

chain in northern Sicily [*Tortorici et al.*, 1995] (Figure 1). As a response to Neogene–Quaternary Africa–Eurasia continental collision and the ongoing southeastwardly subduction of the Ionian plate beneath Calabria, probably associated with the opening of Tyrrhenian Extensional Basin [*Rehault et al.*, 1984; *Malinverno and Ryan*, 1986; *Dewey et al.*, 1989; *Selvaggi and Chiarabba*, 1995; *Gutscher et al.*, 2017], the Calabrian Arc represents one of the most tectonically active regions in the Mediterranean. Since the Pliocene, structural features produced by Neogene shortening have been fragmented by extensional faults producing geomorphological landscapes characterised by structural highs and sedimentary basins [*Barone et al.*, 1982; *Ghisetti and Vezzani*, 1982; *Trincardi and Zitellini*, 1987; *Kastens et al.*, 1988; *Pepe et al.*, 2000, 2003].

Since the Pliocene–Early Pleistocene, Calabria and NE Sicily have been affected by active normal faulting mostly on the Tyrrhenian side and within the Messina Strait between Sicily and Calabria, uplifting and deforming Quaternary marine deposits in response to NW–SE regional extension [*Monaco and Tortorici*, 2000], including near Capo D'Orlando town [*Giunta et al.*, 2012]. Some geoscientists have proposed a cessation or slowing of the roll-back process and associated extension within the Tyrrhenian Basin due to the de-coupling of the Ionian slab from the Calabrian Arc since 700 ky [*Gvirtzman and Nur*, 1999; *Wortel and Spakman*, 2000; *Goes et al.*, 2004; *Serpelloni et al.*, 2005, 2007; *Palano et al.*, 2012]. This suggested slab detachment process is thought to have produced both the sinking of the slab itself, with related isostatic rebound and lithospheric tearing-related faulting near the SW and NE tips of the NW-dipping Ionian slab, producing flow of mantle material through slab windows just beneath the crust of the Calabrian Arc. These processes have produced significant uplift and crustal extension within the upper plate of the Ionian subduction zone through the Middle Pleistocene [*Gvirtzman and Nur*, 1999; *Faccenna et al.*, 2011].

Ongoing extension and uplift is confirmed by (i) GPS investigations, which demonstrate an extension rate of 2 mm/yr with local uplift rates as high as 0.5-1.0 mm/yr [*Serpelloni et al.*, 2005; *Mastrolembo Ventura et al.*, 2014; *Scarfì et al.*, 2016a; *Chiarabba and Palano*, 2017], and (ii) historical seismicity in the overriding plate [*Monaco and Tortorici*, 2000]. Historical damaging earthquakes have been reported in and around the study area [*Guidoboni et al.*, 2007; *Stucchi et al.*, 2013]. In particular, two medium historical seismic events have been located within the investigated area close the Capo

D'Orlando Fault. It remains unclear whether or not the 1613 A.D. Naso earthquake (Mw 5.6, Figure 1) ruptured the Capo D'Orlando Fault or other smaller active faults in its surrounding area (epicentres have been located within five km from the investigated area). Towns such as Naso, Capo D'Orlando and Santa Agata di Militello were shaken by a maximum intensity of IX [*Guidoboni et al.*, 2007], indicating a source fault within a few tens of kilometres or less. A second seismic event, the 1739 A.D. Naso earthquake (Mw 5.1), may also have ruptured Capo d'Orlando Fault or other active faults nearby, because maximum intensities of VIII-IX were recorded [*Guidoboni et al.*, 2007]. Empirically-derived structural parameters such as fault length and expected earthquake magnitude [*Wells and Coppersmith*, 1994; *Galli et al.*, 2008] can be used to suggest that the ~15 km mapped length of the Capo D'Orlando Fault could be capable of producing earthquakes as large as Mw 6, but because the fault length is poorly constrained where it goes offshore in the east, larger magnitudes are not excluded. However, this potential seismogenic structure has not been mapped within the DISS [*Basili et al.*, 2008; *INGV - DISS Working Group*, 2015] although it shows very similar geological/structural parameters to other mapped "debated seismogenic sources" such as the Vibo Valentia Fault and the Taormina Fault which have themselves been mapped through study of Quaternary deformed palaeoshorelines [*Catalano and De Guidi*, 2003; *De Guidi et al.*, 2003; *Tortorici et al.*, 2003; *Bianca et al.*, 2011; *Roberts et al.*, 2013]. We note that the Capo D'Orlando Fault may be capable of hosting surface ruptures to earthquakes, because *Giunta et al.* [2012] report kinematic measurements from a striated fault scarp at outcrop, showing dip slip normal movement (see their inset in their Figure 2), implying slip at the surface rather than activity on a blind fault.

2.2. Late Quaternary palaeoshorelines and existing age controls in the Capo D'Orlando area

The Calabrian Arc has been experiencing uplift above the Ionian subduction zone suggested by the presence of uplifted Quaternary palaeoshorelines and Holocene coastal notches [*Dumas et al.*, 1988, 1993, 2005; *Patacca et al.*, 1990; *Westaway*, 1993; *Miyauchi et al.*, 1994; *Balescu et al.*, 1997; *Stewart et al.*, 1997; *Gvirtzman and Nur*, 1999; *Bonardi et al.*, 2001; *Doglioni et al.*, 2001; *Faccenna et al.*, 2004; *Lucente et al.*, 2006; *Cucci et al.*, 2006; *Ferranti et al.*, 2007; *Bianca et al.*, 2011; *Roberts et al.*,

2013] (Figure 1). Furthermore, as already observed by several geoscientists [*Dumas et al.*, 1981, 1988, *Ghisetti*, 1981, 1984; *Valensise and Pantosti*, 1992; *Westaway*, 1993; *Miyauchi et al.*, 1994; *Bianca et al.*, 1999, 2011; *Catalano and De Guidi*, 2003; *Tortorici et al.*, 2003] the Calabrian Arc provides excellent geological signatures of the interaction between tectonic uplift process and sea-level changes over the Quaternary identified by the presence of dramatic sequences of marine terraces. Here we focus on the fact that tectonically-deformed flights of palaeoshorelines have recorded the effects of Late Quaternary normal faulting activity within the Calabrian Arc [*Jacques et al.*, 2001; *Roberts et al.*, 2013]. In agreement with previous authors [e.g. *Armijo et al.*, 1996; *Bianca et al.*, 2011; *Giunta et al.*, 2012; *Roberts et al.*, 2013] we interpret mapped seaward-sloping marine surfaces as palaeoshoreface surfaces cut by wave-action, with palaeoshorelines at their up-dip, inner edges, which can be traced parallel to the present-day coastline between the towns of Capo D'Orlando and Acquedolci (Figure 2a and 2b). These palaeoshoreface surfaces have been carved into the "Ghiaie di Messina" Formation and, in places, the Mesozoic limestones and/or the Palaeozoic basement (Figure 3). Furthermore, field observations show that in places these palaeosurfaces have been covered by palaeoshoreface deposits such as sandstones and marine conglomerates (Figure 4). In places, we found rounded, marine beach cobbles made of Mesozoic limestone or Palaeozoic crystalline basement as well as borings made by lithophagids affecting the Mesozoic limestones confirming the geological observations of previous authors [*Scicchitano et al.*, 2011; *Giunta et al.*, 2012]. It has been suggested that the Capo D'Orlando Fault has been deforming a partially-dated Late Quaternary sequence of marine terraces in part accommodating the regional extension [*Serpelloni et al.*, 2005; *Mastrolembo Ventura et al.*, 2014; *Scarfi et al.*, 2016b; *Chiarabba and Palano*, 2017], and we investigate this further herein.

Age control on the marine terrace sequence is limited (Table 1), and here we review existing constraints. *Giunta et al.* [2012] used Optically Stimulated Luminescence (OSL) dating of two samples of marine sands associated with two different palaeoshorelines (their II and IV). The more robust of these is sample 23 on palaeoshoreline II, at an elevation of c. 50 m, near the SW fault tip area between Torrenova and Sant'Agata di Militello town (Figure 2a and 2b). This sample shows robust luminescence behaviour, using a widely-applied protocol, and gives an age of 118 ± 7 ka [*Giunta et al.*, 2012], probably indicating the presence of the ~125 ka palaeoshoreline. An *in-situ* shell of *Spondylus* sp. from

sediments just above the marine deposit overlying palaeoshoreline II in the Rocca Scodoni' area was dated by U/Th to c. 125 ka [*Scicchitano et al.*, 2011; *Sulli et al.*, 2013], consistent with the OSL determination. This sequence is located in the hangingwall, close to the centre of the fault if it continues offshore. A further OSL age of 283 ± 22 ka is available from palaeoshoreline IV at 208 m beyond the mapped fault tip close to Fiorita-Sprazzi town (sample 21 in *Giunta et al.* [2012], Figure 2a and 2b). The luminescence characteristics of this sample are not described, but large error bars suggest that the analysis may be close to saturation. Further information would be required to assess the robustness of this age. Other studies have examined a mammal assemblage from deposits at a similar altitude (135 m) to palaeoshoreline III thought to be c. 200 ka old based on isoleucine epimerization dating of bones [*Bada et al.*, 1991]. In this study, we do not use this data point because the stratigraphic link to the marine terrace sequence is tenuous and the method is considered to give relative ages only, despite the attempted quantification.

This paucity of absolute age control for mapped palaeoshorelines near Capo D'Orlando is a typical problem for areas affected by low-uplift rates. Thus, a common problem is how to extrapolate the knowledge of known palaeoshoreline ages to help identify the ages of other un-dated palaeoshorelines. Several authors [e.g. *Bianca et al.*, 1999; *Catalano et al.*, 2003; *Tortorici et al.*, 2003; *Giunta et al.*, 2012; *Gallen et al.*, 2014] have derived uplift rates by applying a sequential correlation approach. This method is based on the idea that, given a dated palaeoshoreline/horizon, the next higher and older palaeoshoreline is likely to belong to the next older sea-level highstand [e.g. *Tortorici et al.*, 2003; *Giunta et al.*, 2012; *Gallen et al.*, 2014]. However, this method can be prone to error if it does not take into account the well-known "overprinting or re-occupation problem" where palaeo-sea-level highstands that have maximum elevations beneath that of subsequent highstands can be overwhelmed by a subsequent, higher palaeo-sea-level highstand; palaeoshoreline indicators from the former can be eroded and not preserved [*Westaway*, 1993; *Roberts et al.*, 2013]. If not considered, the overprinting problem can lead to an erroneous assignment of age. Overprinting is particularly problematic in areas with relatively low uplift rates such as southern Italy [*Westaway*, 1993; *Tortorici et al.*, 2003; *Bianca et al.*, 2011; *Giunta et al.*, 2012; *Roberts et al.*, 2013]. However, *Houghton et al.* [2003] and *Roberts et al.* [2009, 2013] have suggested an alternative approach, whereby an iterative method is used to

calculate all expected palaeoshoreline elevations for a given uplift rate, with all measured palaeoshoreline elevations correlated with all predicted palaeoshoreline elevations synchronously rather than sequentially. An example of this approach was demonstrated using the Vibo Fault, Calabria [*Roberts et al.*, 2013]. Here the 125ka-dated palaeoshoreline was used by previous authors [*Tortorici et al.*, 2003; *Bianca et al.*, 2011] to suggest that the next higher palaeoshoreline belonged to the next older major highstand on the sea-level curve (200 ka), thus deriving a temporally-varying uplift rate. However, *Roberts et al.* [2013] verified the age of the 125ka-dated palaeoshoreline using ^{238}U/^{230}Th of corals that formed part of the terrace, and with this age constraint and application of the synchronous correlation method, they showed that the next higher palaeoshoreline was, instead, the 240 ka marine highstand, resulting in a constant uplift rate throughout the Late Quaternary of 0.75 mm/yr (for detailed reference, see Profile 8 in Figure 2a and table 3 in *Roberts et al.* 2013). This approach takes into account the overprinting problem and is considered here to provide more robust estimates of the uplift history than the sequential approach.

3. Approach and Methods

The study area offers a set of special circumstances that allows investigation of the relationship between regional uplift process and counteracting local tectonics. For example, (i) the Capo D'Orlando normal fault is quasi-parallel to the present-day shoreline, oriented NE–SW, with its displacement decreasing towards the south-west where its tip lies onshore, (ii) hangingwall tectonic subsidence due to normal faulting appears to be slower than the regional uplift process allowing a sequence of marine terraces to be preserved in the hangingwall of the fault, and (iii) the inner edges of the uplifted marine deposits (the palaeoshorelines) can be mapped quasi-parallel to the present-day shoreline. These special circumstances led us to map palaeoshorelines through a detailed DEM-based topographic survey and fieldwork, using existing detailed mapping by *Giunta et al.* [2012] as a guide. We then used a synchronous correlation approach to assign ages to multiple palaeoshorelines, using dating constraints

from previous papers [*Scicchitano et al.*, 2011; *Giunta et al.*, 2012]. We also present previous authors dating for the investigated area (Table 1).

3.1 Palaeoshoreline elevation data: DEM-based topographic analysis and fieldwork

To ensure that we mapped inner edges of marine terraces (palaeoshorelines) which represent the palaeo-sea level related to a highstand, we rely on (i) the presence of key evidence such as lithophagid borings, backshore/foreshore marine deposits containing shallower marine fossils (corals, molluscs, vermetid shells, etc.) as suggested by previous geoscientists [*Ferranti et al.*, 2006; *Roberts et al.*, 2009, 2013; *Giunta et al.*, 2012], and (ii) geomorphic features such as coastal notches [*Boulton and Stewart*, 2015]. In places, the inner edges of marine terraces can be covered by a few meters of younger terrigenous deposits that produce uncertainty regarding the exact palaeoshoreline elevation. However, our mapping shows these are small in vertical extent (a few metres) and hence the uncertainty is likely to have a minimal impact when calculating the implied uplift rates. Inner-edge elevations defining palaeoshorelines for the Capo D'Orlando area were mapped onto a 10-m resolution Digital Elevation Model (DEM) [*Tarquini et al.*, 2007, 2012] and combined, following ground-truthing during fieldwork, with those published by *Giunta et al.* [2012] (Figure 2a). Fifteen topographic profiles, each capturing a sequence of palaeoshorelines, were produced perpendicular to the strike of the fault covering the 15-km extent of the onshore fault (Figure 2b). The topography and presence of preserved palaeoshoreline indicators was used to decide the location of each palaeoshoreline profile; areas of incision caused by rivers were avoided to ensure that the geomorphic features investigated were marine and not fluvial. The presence of palaeoshorelines was confirmed by extensive geological fieldwork during 2015, with elevations determined using a barometric altimeter that we calibrated to elevation benchmarks such as sea-level every few hours. Note that in places we were unable access the palaeoshorelines locations because of thick vegetation and limited access onto private land. However, analysis of DEMs allowed us to map along strike from our field observations and identify palaeoshoreface surface from slightly seaward-sloping surfaces, bounded up-dip by abrupt palaeocliff-like features marking the palaeoshorelines.

3.2 Synchronous correlation approach

The synchronous correlation approach is based on the concept that sea-level highstands, which are thought to produce palaeoshorelines, are unevenly spaced in time, and so for a constant uplift rate, one would expect the palaeoshorelines to be unevenly spaced in elevation. For synchronous correlation, given that at least one palaeoshoreline has age control, the first step is to assume a constant uplift rate and examine whether the implied elevations of palaeoshorelines of different ages match the elevations of measured palaeoshorelines. If they do not, then the uplift-rate can be varied through time and iterated to find the best match with measured palaeoshoreline elevations. This approach was described in detail in *Houghton et al.* [2003] and *Roberts et al.* [2009, 2013].

To implement the synchronous correlation approach, the method is that topographic profiles are constructed across the strike of the palaeoshorelines from DEM data (Figure 5). Then, using fieldwork to ground-truth the profile, interpretations are made of the inner-edge elevations of palaeoshorelines. These elevations are then input into a spreadsheet that is referred to as the Terrace Calculator [*Roberts et al.*, 2009, 2013]. The initial uplift rate for each profile is constrained using one or more dated palaeoshorelines, which is then used to predict the expected elevations for palaeoshoreline of different ages for comparison with measured elevations. R^2 linear regression analysis quantifies the relationship between the predicted and measured inner-edge elevations. The uplift value is iterated to maximise the R^2 value, with values commonly achieved of > 0.99. Where there is no dated surface within a profile, the uplift rates of profiles on either side of the one in question are used to determine the initial uplift value and this was then iterated as described above. Once ages are allocated to all of the palaeoshorelines within the sequence of profiles, a comparison of palaeoshoreline elevations versus age parallel to the strike of the fault is used to determine the extent of the along-strike deformation caused by the fault.

3.3 Footwall palaeoshorelines and long-term uplift/subsidence ratio to derive throw-rate on Capo D'Orlando Fault

Palaeoshorelines have been mapped both on the hangingwall and partially on the footwall of the Capo D'Orlando Fault (see Topographic profile 7, Fig. 6). In particular, a wave cut platform (WCP) cut into limestone associated with Late Quaternary palaeoshoreline deposits has been mapped on its footwall close to the supposed centre of the onshore fault segment at 345 m above sea level (a.s.l) (Figure 2b). Evidence of an upper shoreface marine environment have been recognized such as rounded marine beach cobbles, possible mill-holes and poorly-preserved and hence equivocal lithophagid borings, all of which probably indicate a palaeo-rocky beach. We use the elevations of these footwall wave cut platforms, and their hangingwall equivalents identified mapping around the SW fault tip, to estimate long-term fault displacement by applying a long-term uplift/subsidence ratio proposed by several authors [*King et al.*, 1988; *Armijo et al.*, 1996; *McNeill and Collier*, 2004]. A value of 1/3.5 (uplift/subsidence) ratio has been applied, and we use the elevation of the 340 ka palaeoshoreline mapped close the centre of fault on the hangingwall at 129 m and within the fault "tip zone" at 291 m as being the correlative surface with the lowest WCP on the footwall.

4. Results

First, we show that the approach advocated above can re-produce measured palaeoshoreline elevations by matching them with predicted elevations. We then correlate palaeoshoreline elevations along-strike for the Capo D'Orlando Fault. Finally, we use the derived spatial and temporal constraints on the palaeoshoreline geometries to derive uplift rates and how these relate to displacements on the active normal fault.

We show our synchronous correlation between mapped palaeoshorelines and palaeoshore elevations predicted through iteration of the uplift rate (Figure 6). We iterated the uplift rates to find the best fit between mapped and predicted palaeoshorelines using the dual criteria of (i) making sure that the clearest mapped palaeoshorelines were matched by the most prominent sea-level highstands at 125, 240 and 340 ka, and (ii) maximising the R^2 value that shows how well other less prominent mapped palaeoshorelines match the predicted palaeoshoreline elevations. Through our synchronous correlation we are able to reassess ages for all mapped but un-dated palaeoshorelines (Table 2). It is important to

note that our interpreted palaeo-sea-cliffs defining palaeoshorelines are clear on the DEM. However, in places some of the palaeoshorelines are too small in geographic extent to see at the resolution of the DEM, yet were clear during the fieldwork (Figure 4 for the Profile 6 with the125ka-dated palaeoshoreline clear in the field). Nonetheless, we have indicated these subtle mapped palaeoshorelines and included them in the synchronous correlation (Figure 6). In order to check (a) the correlation between elevations determined from the DEM and those measured with a hand-held barometric altimeter in the field, and (b) how well the measured elevations match the predicted elevations from synchronous correlation (Figure 7). We find that (a) elevations measured on the DEM match those measured in the field within measurement error, suggesting our measured elevations are robust (Figure 7a), and (b) our predicted elevations match the measured ones within error, suggesting we have gained a robust correlation, and reliable uplift-rate estimates (Figure 7b).

The linear regression analysis described above implies a robust, synchronous correlation between multiple sea-level highstands and multiple palaeoshoreline elevations. This key observation also suggests that uplift rates have not fluctuated through time. Another implication is that we have identified palaeoshorelines associated with the sea-level highstands from 76 ka, 100 ka, 125 ka, 175 ka, 200 ka, 217 ka, 240 ka, 285 ka, 310 ka, 340 ka and 410 ka (not all mapped within a single profile) (Table 3); these synchronously-derived ages of palaeoshorelines have been recognised elsewhere in the Mediterranean area [e.g. *Roberts et al.*, 2009, 2013]. Our results also confirm that mapping by *Giunta et al.* [2012] is reliable and robust, but we assign amended ages to his mapped palaeoshorelines.

We use our interpretations between multiple mapped palaeoshorelines and multiple iteratively-predicted highstand elevations to produce a correlation of palaeoshorelines along the strike of the Capo D'Orlando Fault (Figure 8). In particular, our synchronous correlation shows that uplift rates are constant over the Late Quaternary yet vary spatially, with an uplift rate of 0.35 mm/yr in the centre of the hangingwall of the fault, increasing towards the fault tip and beyond where the uplift rate is 0.89 mm/yr (Figure 8a). Because the uplifted palaeoshorelines are in the hangingwall of the Capo D'Orlando Fault, this suggests that finite uplift is a combination of a "regional" uplift signal and local fault-controlled subsidence.

The observation that uplift varies along the strike of the fault, with folded and tilted palaeoshorelines (Figure 8b), suggests that there is a displacement gradient along the fault. We have investigated whether folding and tilting have occurred through time or after formation of all the palaeoshorelines by examining values of tilt along strike and how these vary for different palaeoshoreline ages. If faulting has occurred progressively through time we would expect older palaeoshorelines to be more tilted than younger ones along the strike of the fault. Note that tilt angle values for each investigated palaeoshoreline have been calculated, as a tan^{-1} of a gradient "m" of straight line equation (y=mx). We then show that older and higher mapped palaeoshorelines present higher tilt angle values, implying that they have experienced a longer history of faulting activity (Figure 8c). We interpret this evidence to indicate that faulting has occurred progressively through time, during the progressive formation of successive palaeoshorelines. Our interpretations also reveal another stratigraphic feature consistent with along-strike variation in fault activity rate. The implied increase in uplift rate in the hangingwall of the fault towards the fault tip has allowed more palaeoshorelines to be preserved where the uplift rate is higher (Figure 8b). This fact is to be expected because the overprinting problem mentioned above will destroy some palaeoshorelines if the uplift rate is low. Thus, the increase in the number of palaeoshorelines with uplift rate and increase in tilt angle with age are both diagnostic of incremental fault-controlled deformation, and similar features have been reported for other areas deformed by active normal faults in the Gulf of Corinth [*Armijo et al.*, 1996; *Roberts et al.*, 2009] and the Calabrian Arc [*Roberts et al.*, 2013].

We recognize a "tip zone" defined by (i) higher number of preserved marine terraces, (ii) a shallowing of the long-term tilt angle value recorded by palaeoshorelines from NE to SW and (iii) field-based evidence showing that the fault scarp mapped by Giunta et al. [2012] dies out along strike towards the tip zone (Figure 8b). This "zone" in figure 2b coincides with the red-coloured dashed line in the SW fault tip. This observation provides the opportunity to attempt to correlate hangingwall palaeoshorelines with those on the footwall by mapping them around the fault tip. It, in turn, allows us to calculate the throw-rate on the fault. Our field mapping suggests a correlation between the hangingwall palaeoshoreline that (i) we have assigned to the 340 ka sea-level highstand, and (ii) we have mapped at 291 m in the tip zone, with a footwall palaeoshoreline that we have mapped to the NE in the footwall

at an elevation of 345 m near the middle of the footwall of the fault. In other words, we have been able to correlate a palaeoshoreline across the fault from the hangingwall to the footwall. To gain the rate of vertical offset we have (i) applied a long-term uplift/subsidence ration of 1/3.5 along Profile 7 at the centre of fault, intercepting the WCP mapped in the footwall to predict the footwall elevation of the 340 ka palaeoshoreline, and (ii) taken into account the implied "minimum displacement" (or the hangingwall subsidence) for the 340 ka palaeoshoreline calculated between the hangingwall elevation and the elevation within the fault tip zone (Profile 13). We obtained a "predicted" footwall palaeoshoreline elevation of 335 m which we suggest could be associated with the 345 m high palaeoshoreline that we have mapped in the footwall. The offset between the footwall and the hangingwall implies a constant long-term fault throw-rate of 0.63 ± 0.02 mm/yr derived by a fault throw of 216 m for the last 340 kyrs (Figure 8b). Note that the uncertainty has been estimated by applying a formula to calculate error propagation as follows: $dTR = |TR|*sqrt[(dD/D)^2 + (dt/T)^2]$ where dTR is the calculated uncertainty, TR (0.63 mm/yr) is the throw rate, D (216 m = 216000 mm) is the measured displacement and T (340 kyr = 340000 yr) is the time over the displacement occurred. Furthermore, error value associated with the displacement (dD) is 5000 mm which is derived by barometric altimeter error resolution; error value associated with the age of highstand (dT) is 4000 yr [*Siddall et al.*, 2003; *Rohling et al.*, 2014].

These results confirm that the Capo D'Orlando Fault has been offsetting the investigated palaeoshorelines at the surface throughout the Late Quaternary, proving that this fault is not blind. Our interpretations described above suggest that the regional uplift can be defined within and beyond the tip-zone of the Capo D'Orlando Fault; it is implied that this value is ~ 0.9 mm/yr. However, note that further detailed studies are needed to define whether this candidate value for the regional uplift is in fact influenced by possible active faults offshore.

5. Discussion

In this study, we have investigated the relationship between multiple Late Quaternary palaeoshorelines, active normal faulting and regional uplift. Our results indicate a long-term constant

fault throw-rate and related fault-modified regional uplift rate, rather than an uplift rate that fluctuates through time (Figure 9). Recognition that the Capo D'Orlando Fault has modified the "regional" uplift signal with a constant rate has implications for the geography of the seismic hazard of NE Sicily and within the wider area of the geological domain of the Calabrian Arc (Figure 10). In particular, it implies that slip distributions calculated for subduction interfaces based on uplift data need to consider ongoing crustal deformation within the upper plate. We discuss this in more detail with regard to local and regional processes.

5.1. Local tectonic implications: estimating fault throw-rate and Earthquake Recurrence Interval for the Capo D'Orlando Fault

At the local scale, the investigated area shows clear evidence that the uplift rate field varies along strike of the Capo D'Orlando Fault (Figure 8a), indicating that this normal fault is active. This fact is not surprising considering that NE Sicily has been affected by historical damaging earthquakes (Figure 1). Therefore, we suggest that the Capo D'Orlando Fault should be added within DISS at least as "Debated Seismogenic Source" to improve the seismic hazard assessment for the NE Sicily.

For the Capo D'Orlando Fault, we suggest a constant throw-rate of 0.63 ± 0.02 mm/yr on the as the most likely scenario by investigating fault-deformed Late Quaternary palaeoshorelines outcropping in the hangingwall and footwall of this fault (Figure 9). The throw-rate value is not unusual considering that slip-rate values measured for other active normal faults which have been accommodating the Plio-Pleistocene crustal extension along the Italian Apennines and the Calabrian Arc are within the range 0.3 mm/yr to 2.0 mm/yr [*Jacques et al.*, 2001; *Galli and Bosi*, 2002; *Roberts and Michetti*, 2004]. Also, well-known empirical correlations between fault length, maximum expected magnitude and maximum expected displacement [*Wells and Coppersmith*, 1994; *Galli et al.*, 2008] allow us to calculate, for the first time, an estimated earthquake recurrence interval or T_{mean} for the Capo D'Orlando Fault which, considering the length of the fault mapped onshore, could be capable of earthquakes with maximum magnitude (M) of 6.2. To produce a fault throw-rate of 0.63 ± 0.02 mm/yr given 50 cm maximum vertical slip events in Mw 6.2 earthquakes implies an earthquake recurrence

interval of 820 years; this value is comparable to those that characterize active normal faults along the Italian peninsula [*Jacques et al.*, 2001; *Galli et al.*, 2008; *Roberts et al.*, 2013]. However, the NE tip of the fault has not identified because hangingwall uplift (that is hangingwall subsidence plus regional uplift) is still low relative to the tip zone that has been identified at the SW end of the fault (Figure 8). We suggest that the NE fault tip is likely to be offshore, implying a longer fault length. If the Capo D'Orlando Fault is longer than 15 km, this increases the possible maximum earthquake magnitude to > Mw 6.2; in turn, it implies larger slip events and hence longer earthquake recurrence intervals, suggesting that further study of the offshore are needed. We point out that we have explored a scenario using a possible maximum magnitude earthquake, assuming that earthquakes rupture along the entire length of the Capo D'Orlando Fault; shorter recurrence intervals are implied if only part of the fault length ruptures.

5.2. Crustal deformation within the upper plate of the Ionian subduction zone: regional tectonic implications, slip distribution calculations, mantle-related uplift and the associated seismic hazard on subduction zones

Our study shows that the "regional" uplift signal, within the upper plate of the Ionian subduction zone since the Late Quaternary, has been spatially perturbed by "local" crustal deformation that needs to be considered to attempt long-term seismic hazard assessment.

Generally, it is common to infer slip distributions on the subduction interface and mantle upwelling processes from observations of uplift in the upper plate of the subduction zone *[e.g. Gvirtzman and Nur, 1999; Wortel and Spakman 2000; D'Agostino et al., 2001; McCloskey et al., 2005; Meltzner et al., 2006; Faure Walker et al., 2012; Nalbant et al., 2013; Nic Bhloscaidh et al., 2015].* The Ionian subduction associated with roll-back of the Ionian slab [*Goes et al.*, 2004], and asthenospheric upwelling beneath the continental crust of the Calabrian Arc [*Gvirtzman and Nur*, 1999; *Wortel and Spakman*, 2000] has occurred synchronously with uplift of the Calabrian forearc over the Late Quaternary. However, we emphasise that the Calabrian Arc shows prominent intra-crustal

deformation mostly in the form of active normal faulting controlling the topography of the area (Figure 10). In particular, topographic highs exist due to tectonic uplift in the footwalls of active normal faults such as the Maratea Fault [e.g. *Papanikolaou and Roberts*, 2007], the Pollino Fault [e.g. *Michetti et al.*, 1997], the Vibo Fault [e.g. *Roberts et al.*, 2013], the Cittanova Fault [e.g. *Jacques et al.*, 2001; *Galli and Bosi*, 2002; *Roda-Boluda and Whittaker*, 2017], the Taormina Fault [e.g. *Catalano and De Guidi*, 2003; *De Guidi et al.*, 2003; *Spampinato et al.*, 2012] and the Capo D'Orlando Fault itself [e.g. *Scicchitano et al.*, 2011; *Giunta et al.*, 2012 and this study] (Figure 1). These faults have been seismically deforming the upper plate of the Ionian subduction zone producing damaging earthquakes. Spatial variation in uplift rates measured over (i) the Late Quaternary [*Antonioli et al.*, 2006, 2009; *Ferranti et al.*, 2006; *Roberts et al.*, 2013 and this study] and (ii) the last decades shown by using GPS analysis [*Serpelloni et al.*, 2013] along the strike of these faults (Figure 10a and 10b) imply that uplift is not simply controlled either by slip on the subduction interfaces or mantle upwelling-related dynamic topography; the upper plate seismogenic sources will strongly affect the "regional" uplift over wavelengths of a few tens of kilometres within the Calabrian Arc, implying that these normal faults need to be well-defined. We suggest that differential uplift due to the "local effect" of normal faulting has been occurring through time along the Calabrian forearc (Figure 8 and 9). Therefore, if the variation in uplift rates due to these normal faults is not recognised and removed from calculations, this could lead to (i) overly complicated and misleading subduction interface slip distributions and (ii) erroneous conclusions about the dynamic topography, due to the mantle upwelling [*D'Agostino et al.*, 2001; *Faure Walker et al.*, 2012]. We emphasise that such upper plate normal faulting is widespread with clear examples in central Greece and Crete, Japan and south America [*Armijo et al.*, 1996; *Hasegawa et al.*, 2000; *Saillard et al.*, 2011; *Vacchi et al.*, 2012; *Gallen et al.*, 2014; *Binnie et al.*, 2016]. One finding that is now emerging is that for at least some upper plate normal faults, the throw-rate on the fault through the Late Quaternary is constant through time (e.g. 0.63 ± 0.02 mm/yr from this study), rather than fluctuating through time [e.g. *Giunta et al.*, 2012] (Figure 9). For example, a constant throw-rate through the late Quaternary has also been reported for the Vibo Fault, within the Calabrian Arc [*Roberts et al.* 2013]. If this is common it is implied that constant values of uplift through time need to be

subtracted from regional uplift-rate signals if subduction zone slip distributions and mantle dynamics are to be inferred.

Turning to the regional contribution of the Capo D'Orlando Fault to the regional extension, we suggest that in order to accommodate geodetically-derived regional extension rates of ~2 mm/yr [*Serpelloni et al.*, 2005] or ~3 mm/yr [*Mastrolembo Ventura et al.*, 2014] a well-constrained long-term constant throw-rate through time on the Capo D'Orlando Fault of 0.63 ± 0.02 mm/yr implies that additional crustal deformation has to be accommodated by other active faults across strike. It also perhaps implies that faults across strike will also need to remain active through time to maintain constant throw-rates and hence slip-rates [e.g. *Roberts et al.*, 2002]. Seismic profiles quasi-perpendicular to the coastline of Capo D'Orlando area have already shown offshore crustal extensional processes due to normal faulting [*Nigro and Sulli*, 1995]. It would be interesting to see whether these faults also have constant slip-rates.

However, note that in other locations, active fault systems have been shown to be accommodating crustal deformation with associated rates varying through time. For instance, tectonically-deformed uplifted marine terraces have been investigated within the Gulf of Corinth in Greece [*Roberts et al.*, 2009] who suggest varying long-term fault slip-rates, implying a synchronous change in faulting activity on active faults across strike. In particular, the investigated South Alkyonides active fault in the Gulf of Corinth, Greece, has accelerated its slip-rate synchronous with a deceleration on other faults located across strike over the Late Quaternary [*Roberts et al.*, 2009]. This evidence suggests that when active faults are arranged across strike and interacting, activity can swap back and forth through time on a multi-millenium timescale to accommodate the regional deformation [*Roberts et al.*, 2002; *Bennett et al.*, 2004; *Cowie et al.*, 2005; *Dolan et al.*, 2007; *Nixon et al.*, 2016]. We stress that more studies are needed to better identify the locations long-term crustal deformation, and how they change through time, by studying (i) sequences of tectonically-deformed Late Quaternary marine terraces onshore and (ii) seismic profiles to define faulting activity offshore the investigated area.

Overall, we suggest that local deformation rates measured over the Late Quaternary on upper plate normal faults provide important insights into the subduction process. The deformation within the

upper plate must be subtracted to derive a better understanding of subduction and mantle upwelling, and allow calculation of more robust slip distributions for subduction interface events to feed into seismic hazard analysis associated with subduction-related earthquakes. This knowledge help to understand the seismic hazard related to the upper plate of the Ionian subduction zone in southern Italy.

6. Conclusion

In this paper, we report constant crustal deformation rates through time on a normal fault within the upper plate of the Ionian subduction zone. Late Quaternary palaeoshorelines deformed by the Capo D'Orlando Fault have been investigated by applying a synchronous correlations method. The study shows that the Capo D'Orlando Fault is an active and potential seismic source with a throw-rate of 0.63 $\pm$ 0.02 mm/yr that has been constant through the late Quaternary. In particular, we show that fault displacements have folded and tilted the investigated palaeoshorelines along the strike of the fault, and that higher and older palaeoshorelines have experienced a longer faulting history. The deformed palaeoshorelines demonstrate that the Capo D'Orlando fault is active and should be included in seismic hazard assessments of NE Sicily. The throw-rate of 0.63 $\pm$ 0.02 mm/yr has been constant through time showing that other unidentified active faults are needed to explain the observed 2-3 mm/yr of regional extension measured with GPS. The results suggest that care is needed to include or exclude upper plate deformation, using surface uplift data, when inferring (i) mantle upwelling-related dynamic topography and (ii) slip distributions on subduction interfaces.

All data for this paper are properly cited and referred to in the reference list and available on Figure 6 as topographic data where palaeoshoreline elevations have been mapped and in Table 2. These data can be used to re-produce Results shown in Figure 7, 8 and 9. They are also available by contacting the corresponding author (marco.meschis.14@ucl.ac.uk or marco.meschis@gmail.com).

References

Antonioli, F., S. Kershaw, P. Renda, D. Rust, G. Belluomini, M. Cerasoli, U. Radtke, and S. Silenzi (2006a), Elevation of the last interglacial highstand in Sicily (Italy): A benchmark of coastal tectonics, *Quat. Int.*, *145–146*, 3–18, doi:10.1016/j.quaint.2005.07.002.

Antonioli, F., L. Ferranti, K. Lambeck, S. Kershaw, V. Verrubbi, and G. Dai Pra (2006b), Late Pleistocene to Holocene record of changing uplift rates in southern Calabria and northeastern Sicily (southern Italy, Central Mediterranean Sea), *Tectonophysics*, *422*(1–4), 23–40, doi:10.1016/j.tecto.2006.05.003.

Antonioli, F. et al. (2009), Holocene relative sea-level changes and vertical movements along the Italian and Istrian coastlines, *Quat. Int.*, *206*(1–2), 102–133, doi:10.1016/j.quaint.2008.11.008.

Armijo, R., H. Lyon-Caen, and D. Papanastassiou (1992), East-west extension and Holocene normal-fault scarps in the Hellenic arc, *Geology*, *20*(6), 491–494, doi:10.1130/0091-7613(1992)020<0491:EWEAHN>2.3.CO;2.

Armijo, R., B. Meyer, G. C. P. King, A. Rigo, and D. Papanastassiou (1996), Quaternary evolution of the Corinth Rift and its implications for the Late Cenozoic evolution of the Aegean, *Geophys. J. Int.*, *126*(1), 11–53, doi:10.1111/j.1365-246X.1996.tb05264.x.

Bada, J. L., G. Belluomini, L. Bonfiglio, M. Branca, E. Burgio, and L. Delitala (1991), Isoleucine epimerization ages of Quaternary mammals from Sicily, *Quat.*, *4*, 49–54.

Balescu, S., B. Dumas, P. Guérémy, M. Lamothe, R. Lhénaff, and J. Raffy (1997), Thermoluminescence dating tests of Pleistocene sediments from uplifted marine shorelines along the southwest coastline of the Calabrian Peninsula (southern Italy), *Palaeogeogr. Palaeoclimatol. Palaeoecol.*, *130*(1–4), 25–41, doi:10.1016/S0031-0182(96)00119-8.

Barone, A., A. Fabbri, S. Rossi, and R. Sartori (1982), Geological structure and evolution of the

marine areas adjacent to the Calabrian Arc, *Earth Evol. Sci*, *3*, 207–221.

Basili, R., G. Valensise, P. Vannoli, P. Burrato, U. Fracassi, S. Mariano, M. M. Tiberti, and E. Boschi (2008), The Database of Individual Seismogenic Sources (DISS), version 3: Summarizing 20 years of research on Italy's earthquake geology, *Tectonophysics*, *453*(1–4), 20–43, doi:10.1016/j.tecto.2007.04.014.

Bennett, R. A., A. M. Friedrich, and K. P. Furlong (2004), Codependent histories of the San Andreas and San Jacinto fault zones from inversion of fault displacement rates, *Geology*, *32*(11), 961, doi:10.1130/G20806.1.

Bianca, M., C. Monaco, L. Tortorici, and L. Cernobori (1999), Quaternary normal faulting in southeastern Sicily (Italy): a seismic source for the 1693 large earthquake, *Geophys. J. Int.*, *139*(2), 370–394, doi:10.1046/j.1365-246x.1999.00942.x.

Bianca, M., S. Catalano, G. De Guidi, A. . Gueli, C. Monaco, G. M. Ristuccia, G. Stella, G. Tortorici, L. Tortorici, and S. O. Troja (2011), Luminescence chronology of Pleistocene marine terraces of Capo Vaticano peninsula (Calabria, Southern Italy), *Quat. Int.*, *232*(1–2), 114–121, doi:10.1016/j.quaint.2010.07.013.

Binnie, A., T. J. Dunai, S. A. Binnie, P. Victor, G. González, and A. Bolten (2016), Accelerated late quaternary uplift revealed by 10 Be exposure dating of marine terraces, Mejillones Peninsula, northern Chile, *Quat. Geochronol.*, *36*, 12–27, doi:10.1016/j.quageo.2016.06.005.

Bonardi, G., W. Cavazza, V. Perrone, and S. Rossi (2001), Calabria-Peloritani terrane and northern Ionian sea, in *Anatomy of an Orogen: The apennines and adjacent mediterranean basins*, pp. 287–306, Springer.

Boulton, S. J., and I. S. Stewart (2015), Holocene coastal notches in the Mediterranean region: Indicators of palaeoseismic clustering?, *Geomorphology*, *237*, 29–37, doi:10.1016/j.geomorph.2013.11.012.

Catalano, S., and G. De Guidi (2003), Late Quaternary uplift of northeastern Sicily: Relation with the active normal faulting deformation, *J. Geodyn.*, *36*(4), 445–467, doi:10.1016/S0264-3707(02)00035-2.

Catalano, S., G. De Guidi, C. Monaco, G. Tortorici, and L. Tortorici (2003), Long-term behaviour of

the late Quaternary normal faults in the Straits of Messina area (Calabrian arc): Structural and morphological constraints, *Quat. Int.*, *101–102*(1), 81–91, doi:10.1016/S1040-6182(02)00091-5.

Chapman, N., K. Berryman, P. Villamor, W. Epstein, L. Cluff, and H. Kawamura (2014), Active Faults and Nuclear Power Plants, *Eos, Trans. Am. Geophys. Union*, *95*(4), 33–34, doi:10.1002/2014EO040001.

Chiarabba, C., and M. Palano (2017), Progressive migration of slab break-off along the southern Tyrrhenian plate boundary: Constraints for the present day kinematics, *J. Geodyn.*, *105*, 51–61, doi:https://doi.org/10.1016/j.jog.2017.01.006.

Cowie, P., J. Underhill, M. Behn, J. Lin, and C. Gill (2005), Spatio-temporal evolution of strain accumulation derived from multi-scale observations of Late Jurassic rifting in the northern North Sea: A critical test of models for lithospheric extension, *Earth Planet. Sci. Lett.*, *234*(3–4), 401–419, doi:10.1016/j.epsl.2005.01.039.

Cowie, P. a., G. P. Roberts, J. M. Bull, and F. Visini (2012), Relationships between fault geometry, slip rate variability and earthquake recurrence in extensional settings, *Geophys. J. Int.*, *189*(1), 143–160, doi:10.1111/j.1365-246X.2012.05378.x.

Cucci, L., A. Tertulliani, I. Nazionale, S. Sismologia, and V. Murata (2006), I Terrazzi Marini Nell ’ Area Di Capo Vaticano (Arco Calabro): Solo Un Record Di Sollevamento Regionale O Anche Di Deformazione Cosismica ?, *Quat.*, *19*(1), 89–101.

D’Agostino, N., J. A. Jackson, F. Dramis, and R. Funiciello (2001), Interactions between mantle upwelling, drainage evolution and active normal faulting: an example from the central Apennines (Italy), *Geophys. J. Int.*, *147*(2), 475–497, doi:10.1046/j.1365-246X.2001.00539.x.

Dewey, J. F., M. L. Helman, S. D. Knott, E. Turco, and D. H. W. Hutton (1989), Kinematics of the western Mediterranean, *Geol. Soc. London, Spec. Publ.*, *45*(1), 265–283, doi:10.1144/GSL.SP.1989.045.01.15.

Doglioni, C., F. Innocenti, and G. Mariotti (2001), Why Mt Etna ?, *Terra Nov.*, *13*, 25–31.

Dolan, J. F., D. D. Bowman, and C. G. Sammis (2007), Long-range and long-term fault interactions in Southern California, *Geology*, *35*(9), 855–858, doi:10.1130/G23789A.1.

Dumas, B., P. Gueremy, R. Lhenaff, and J. Raffy (1981), Le soulèvement quaternaire de la Calabre

méridionale, *Rev. Géologie Dyn. Géographie Phys. Paris*, *23*, 27–40.

Dumas, B., P. Gueremy, P. J. Hearty, R. Lhenaff, and J. Raffy (1988), Morphometric analysis and amino acid geochronology of uplifted shorelines in a tectonic region near reggio Calambria, South Italy, *Palaeogeogr. Palaeoclimatol. Palaeoecol.*, *68*(2–4), 273–289, doi:10.1016/0031-0182(88)90045-4.

Dumas, B., P. Gueremy, R. Lhenaff, and J. Raffy (1993), Rapid uplift, stepped marine terraces and raised shorelines on the Calabrian coast of Messina Strait, Italy, *Earth Surf. Process. Landforms*, *18*(3), 241–256, doi:10.1002/esp.3290180306.

Dumas, B., P. Guérémy, and J. Raffy (2005), Evidence for sea-level oscillations by the "characteristic thickness" of marine deposits from raised terraces of Southern Calabria (Italy), *Quat. Sci. Rev.*, *24*(18–19), 2120–2136, doi:10.1016/j.quascirev.2004.12.011.

Faccenna, C., C. Piromallo, A. Crespo-Blanc, L. Jolivet, and F. Rossetti (2004), Lateral slab deformation and the origin of the western Mediterranean arcs, *Tectonics*, *23*(1), n/a-n/a, doi:10.1029/2002TC001488.

Faccenna, C., P. Molin, B. Orecchio, V. Olivetti, O. Bellier, F. Funiciello, L. Minelli, C. Piromallo, and A. Billi (2011), Topography of the Calabria subduction zone (southern Italy): Clues for the origin of Mt. Etna, *Tectonics*, *30*(1), 1–20, doi:10.1029/2010TC002694.

Faccenna, C., T. W. Becker, M. S. Miller, E. Serpelloni, and S. D. Willett (2014), Isostasy, dynamic topography, and the elevation of the Apennines of Italy, *Earth Planet. Sci. Lett.*, *407*, 163–174, doi:10.1016/j.epsl.2014.09.027.

Faure Walker, J. P., G. P. Roberts, P. R. Sammonds, and P. Cowie (2010), Comparison of earthquake strains over 10 2 and 10 4 year timescales: Insights into variability in the seismic cycle in the central Apennines, Italy, *J. Geophys. Res.*, *115*(B10), B10418, doi:10.1029/2009JB006462.

Faure Walker, J. P., G. P. Roberts, P. A. Cowie, I. Papanikolaou, A. M. Michetti, P. Sammonds, M. Wilkinson, K. J. W. McCaffrey, and R. J. Phillips (2012), Relationship between topography, rates of extension and mantle dynamics in the actively-extending Italian Apennines, *Earth Planet. Sci. Lett.*, *325–326*, 76–84, doi:10.1016/j.epsl.2012.01.028.

Ferranti, L. et al. (2006), Markers of the last interglacial sea-level high stand along the coast of Italy:

Tectonic implications, *Quat. Int.*, *145–146*, 30–54, doi:10.1016/j.quaint.2005.07.009.

Ferranti, L., C. Monaco, F. Antonioli, L. Maschio, S. Kershaw, and V. Verrubbi (2007), The contribution of regional uplift and coseismic slip to the vertical crustal motion in the Messina Straits, southern Italy: Evidence from raised Late Holocene shorelines, *J. Geophys. Res.*, *112*(B6), B06401, doi:10.1029/2006JB004473.

Friedrich, A. M., B. P. Wernicke, N. A. Niemi, R. A. Bennett, and J. L. Davis (2003), Comparison of geodetic and geologic data from the Wasatch region, Utah, and implications for the spectral character of Earth deformation at periods of 10 to 10 million years, *J. Geophys. Res. Solid Earth*, *108*(B4), 2199, doi:10.1029/2001JB000682.

Gallen, S. F., K. W. Wegmann, D. R. Bohnenstiehl, F. J. Pazzaglia, M. T. Brandon, and C. Fassoulas (2014), Active simultaneous uplift and margin-normal extension in a forearc high, Crete, Greece, *Earth Planet. Sci. Lett.*, *398*, 11–24, doi:10.1016/j.epsl.2014.04.038.

Galli, P., and V. Bosi (2002), Paleoseismology along the Cittanova fault: Implications for seismotectonics and earthquake recurrence in Calabria (southern Italy), *J. Geophys. Res.*, *107*(B3), 2044, doi:10.1029/2001JB000234.

Galli, P., F. Galadini, and D. Pantosti (2008), Twenty years of paleoseismology in Italy, *Earth-Science Rev.*, *88*(1–2), 89–117, doi:10.1016/j.earscirev.2008.01.001.

Ghisetti, F. (1981), Upper Pliocene-Pleistocene uplift rates as indicators of neotectonic pattern: an example from southern Calabria (Italy), *Z. Geomorphol*, *40*, 93–118.

Ghisetti, F. (1984), Recent deformations and the seismogenic source in the Messina Strait (southern Italy), , *109*, 191–208, doi:https://doi.org/10.1016/0040-1951(84)90140-9.

Ghisetti, F., and L. Vezzani (1982), Different styles of deformation in the calabrian arc (Southern Italy): Implications for a seismotectonic zoning, *Tectonophysics*, *85*(3–4), 149–165, doi:10.1016/0040-1951(82)90101-9.

Giunta, G., A. M. Gueli, C. Monaco, S. Orioli, G. M. Ristuccia, G. Stella, and S. O. Troja (2012), Middle-Late Pleistocene marine terraces and fault activity in the Sant'Agata di Militello coastal area (north-eastern Sicily), *J. Geodyn.*, *55*, 32–40, doi:10.1016/j.jog.2011.11.005.

Goes, S., D. Giardini, S. Jenny, C. Hollenstein, H.-G. Kahle, and A. Geiger (2004), A recent tectonic

reorganization in the south-central Mediterranean, *Earth Planet. Sci. Lett.*, *226*(3–4), 335–345, doi:10.1016/j.epsl.2004.07.038.

De Guidi, G., S. Catalano, C. Monaco, and L. Tortorici (2003), Morphological evidence of Holocene coseismic deformation in the Taormina region (NE Sicily), *J. Geodyn.*, *36*(1–2), 193–211, doi:10.1016/S0264-3707(03)00047-4.

Guidoboni, E., G. Ferrari, D. Mariotti, A. Comastri, G. Tarabusi, and G. Valensise (2007), Catalogue of Strong Earthquakes in Italy (461 BC-1997) and Mediterranean Area (760 BC-1500),

Gutscher, M.-A. et al. (2017), Active tectonics of the Calabrian subduction revealed by new multi-beam bathymetric data and high-resolution seismic profiles in the Ionian Sea (Central Mediterranean), *Earth Planet. Sci. Lett.*, *461*, 61–72, doi:10.1016/j.epsl.2016.12.020.

Gvirtzman, Z., and A. Nur (1999), The formation of Mount Etna as the consequence of slab rollback, *Nature*, *401*(October), 782–785, doi:10.1038/44555.

Hasegawa, A., A. Yamamoto, N. Umino, S. Miura, S. Horiuchi, D. Zhao, and H. Sato (2000), Seismic activity and deformation process of the overriding plate in the northeastern Japan subduction zone, *Tectonophysics*, *319*(4), 225–239, doi:10.1016/S0040-1951(99)00296-6.

Houghton, S. L., G. P. Roberts, I. D. Papanikolaou, and J. M. McArthur (2003), New 234 U- 230 Th coral dates from the western Gulf of Corinth: Implications for extensional tectonics, *Geophys. Res. Lett.*, *30*(19), 2013, doi:10.1029/2003GL018112.

INGV - DISS Working Group (2015), Database of Individual Seismogenic Sources (DISS), Version 3.2.0: A compilation of potential sources for earthquakes larger than M 5.5 in Italy and surrounding areas, , doi:10.6092/INGV.IT-DISS3.2.0.

Jacques, E., C. Monaco, P. Tapponnier, L. Tortorici, and T. Winter (2001), Faulting and earthquake triggering during the 1783 Calabria seismic sequence, *Geophys. J. Int.*, *147*(3), 499–516, doi:10.1046/j.0956-540x.2001.01518.x.

Kastens, K. et al. (1988), ODP Leg 107 in the Tyrrhenian Sea: Insights into passive margin and back-arc basin evolution, *Geol. Soc. Am. Bull.*, *100*(7), 1140–1156, doi:10.1130/0016-7606(1988)100<1140:OLITTS>2.3.CO;2.

King, G. C. P., R. S. Stein, and J. B. Rundle (1988), The Growth of Geological Structures by

Repeated Earthquakes 1. Conceptual Framework, *J. Geophys. Res. Solid Earth*, *93*(B11), 13307–13318, doi:10.1029/JB093iB11p13307.

Lucente, F. P., L. Margheriti, C. Piromallo, and G. Barruol (2006), Seismic anisotropy reveals the long route of the slab through the western-central Mediterranean mantle, *Earth Planet. Sci. Lett.*, *241*(3–4), 517–529, doi:10.1016/j.epsl.2005.10.041.

Malinverno, A., and W. B. F. Ryan (1986), Extension in the Tyrrhenian Sea and shortening in the Apennines as result of arc migration driven by sinking of the lithosphere, *Tectonics*, *5*(2), 227–245, doi:10.1029/TC005i002p00227.

Massonnet, D., and K. L. Feigl (1995), Satellite radar interferometric map of the coseismic deformation field of the M = 6.1 Eureka Valley, California Earthquake of May 17, 1993, *Geophys. Res. Lett.*, *22*(12), 1541–1544, doi:10.1029/95GL01088.

Massonnet, D., M. Rossi, C. Carmona, F. Adragna, G. Peltzer, K. Feigl, and T. Rabaute (1993), The displacement field of the Landers earthquake mapped by radar interferometry, *Nature*, *364*(6433), 138–142, doi:10.1038/364138a0.

Mastrolembo Ventura, B., E. Serpelloni, A. Argnani, A. Bonforte, R. Bürgmann, M. Anzidei, P. Baldi, and G. Puglisi (2014), Fast geodetic strain-rates in eastern Sicily (southern Italy): New insights into block tectonics and seismic potential in the area of the great 1693 earthquake, *Earth Planet. Sci. Lett.*, *404*, 77–88, doi:10.1016/j.epsl.2014.07.025.

McCloskey, J., S. S. Nalbant, and S. Steacy (2005), Indonesian earthquake: Earthquake risk from co-seismic stress, *Nature*, *434*(7031), 291–291, doi:10.1038/434291a.

McNeill, L. C., and R. E. L. Collier (2004), Uplift and slip rates of the eastern Eliki fault segment, Gulf of Corinth, Greece, inferred from Holocene and Pleistocene terraces, *J. Geol. Soc. London.*, *161*(1), 81–92, doi:10.1144/0016-764903-029.

Meltzner, A. J., K. Sieh, M. Abrams, D. C. Agnew, K. W. Hudnut, J.-P. Avouac, and D. H. Natawidjaja (2006), Uplift and subsidence associated with the great Aceh-Andaman earthquake of 2004, *J. Geophys. Res. Solid Earth*, *111*(B2), n/a-n/a, doi:10.1029/2005JB003891.

Michetti, A. M., L. Ferreli, L. Serva, and E. Vittori (1997), Geological evidence for strong historical earthquakes in an "aseismic" region: The Pollino case (Southern Italy), *J. Geodyn.*, *24*(1–4), 67–

86, doi:10.1016/S0264-3707(97)00018-5.

Miyauchi, T., G. Dai Pra, and S. Sylos Labini (1994), Geochronology of Pleistocene marine terraces and regional tectonics in the Tyrrhenian coast of South Calabria, Italy, *Quat.*, *7*, 17–34.

Monaco, C., and L. Tortorici (2000), Active faulting in the Calabrian arc and eastern Sicily, *J. Geodyn.*, *29*(3–5), 407–424, doi:10.1016/S0264-3707(99)00052-6.

Nalbant, S., J. McCloskey, S. Steacy, M. NicBhloscaidh, and S. Murphy (2013), Interseismic coupling, stress evolution, and earthquake slip on the Sunda megathrust, *Geophys. Res. Lett.*, *40*(16), 4204–4208, doi:10.1002/grl.50776.

Nic Bhloscaidh, M., J. McCloskey, M. Naylor, S. Murphy, and A. Lindsay (2015), Reconstruction of the slip distributions in historical earthquakes on the Sunda megathrust, W. Sumatra, *Geophys. J. Int.*, *202*(2), 1339–1361, doi:10.1093/gji/ggv195.

Nicol, A., and J. Beavan (2003), Shortening of an overriding plate and its implications for slip on a subduction thrust, central Hikurangi Margin, New Zealand, *Tectonics*, *22*(6), n/a-n/a, doi:10.1029/2003TC001521.

Nigro, F., and A. Sulli (1995), Plio-Pleistocene extensional tectonics in the Western Peloritani area and its offshore (northeastern Sicily), *Tectonophysics*, *252*(1–4), 295–305, doi:10.1016/0040-1951(95)00096-8.

Nixon, C. W. et al. (2016), Rapid spatiotemporal variations in rift structure during development of the Corinth Rift, central Greece, *Tectonics*, *35*(5), 1225–1248, doi:10.1002/2015TC004026.

Palano, M., L. Ferranti, C. Monaco, M. Mattia, M. Aloisi, V. Bruno, F. Cannav??, and G. Siligato (2012), GPS velocity and strain fields in Sicily and southern Calabria, Italy: Updated geodetic constraints on tectonic block interaction in the central Mediterranean, *Rend. Online Soc. Geol. Ital.*, *21*(PART 1), 235–237, doi:10.1029/2012JB009254.

Papanikolaou, D., M. Alexandri, and P. Nomikou (2006), Active faulting in the north Aegean basin, in *Special Paper 409: Postcollisional Tectonics and Magmatism in the Mediterranean Region and Asia*, pp. 189–209, Geological Society of America.

Papanikolaou, I. D., and G. P. Roberts (2007), Geometry, kinematics and deformation rates along the active normal fault system in the southern Apennines: Implications for fault growth, *J. Struct.*

Geol., *29*(1), 166–188, doi:10.1016/j.jsg.2006.07.009.

Papanikolaou, I. D., G. P. Roberts, and A. M. Michetti (2005), Fault scarps and deformation rates in

Lazio–Abruzzo, Central Italy: Comparison between geological fault slip-rate and GPS data,

Tectonophysics, *408*(1–4), 147–176, doi:10.1016/j.tecto.2005.05.043.

Papanikolaou, I. D., M. Foumelis, I. Parcharidis, E. L. Lekkas, and I. G. Fountoulis (2010),

Deformation pattern of the 6 and 7 April 2009, M_W=6.3 and M_W=5.6 earthquakes in L'Aquila

(Central Italy) revealed by ground and space based observations, *Nat. Hazards Earth Syst. Sci.*,

10(1), 73–87, doi:10.5194/nhess-10-73-2010.

Patacca, E., R. Sartori, and P. Scandone (1990), Tyrrenian basin and apenninic arcs: kinematic

relations since late Tortonian times, *Mem. della Soc. Geol. Ital.*, *45*, 425–451.

Pepe, F., G. Bertotti, F. Cella, and E. Marsella (2000), Rifted margin formation in the south

Tyrrhenian Sea: A high-resolution seismic profile across the north Sicily passive continental

margin, *Tectonics*, *19*(2), 241–257, doi:10.1029/1999TC900067.

Pepe, F., A. Sulli, M. Agate, D. Di Maio, A. Kok, C. Lo Iacono, and R. Catalano (2003), Plio-

Pleistocene geological evolution of the northern Sicily continental margin (southern Tyrrhenian

Sea): new insights from high-resolution, multi-electrode sparker profiles, *Geo-Marine Lett.*,

23(1), 53–63, doi:10.1007/s00367-003-0124-3.

Rehault, J.-P., G. Boillot, and A. Mauffret (1984), The Western Mediterranean Basin geological

evolution, *Mar. Geol.*, *55*(3–4), 447–477, doi:10.1016/0025-3227(84)90081-1.

Roberts, G. P., and A. M. Michetti (2004), Spatial and temporal variations in growth rates along

active normal fault systems: an example from The Lazio–Abruzzo Apennines, central Italy, *J.

Struct. Geol.*, *26*(2), 339–376, doi:10.1016/S0191-8141(03)00103-2.

Roberts, G. P., A. M. Michetti, P. Cowie, N. C. Morewood, and I. Papanikolaou (2002), Fault slip-

rate variations during crustal-scale strain localisation, central Italy, *Geophys. Res. Lett.*, *29*(8), 9-

1-9–4, doi:10.1029/2001GL013529.

Roberts, G. P., S. L. Houghton, C. Underwood, I. Papanikolaou, P. A. Cowie, P. van Calsteren, T.

Wigley, F. J. Cooper, and J. M. McArthur (2009), Localization of Quaternary slip rates in an

active rift in 10 5 years: An example from central Greece constrained by 234 U- 230 Th coral

dates from uplifted paleoshorelines, *J. Geophys. Res.*, *114*(B10), B10406, doi:10.1029/2008JB005818.

Roberts, G. P., M. Meschis, S. Houghton, C. Underwood, and R. M. Briant (2013), The implications of revised Quaternary palaeoshoreline chronologies for the rates of active extension and uplift in the upper plate of subduction zones, *Quat. Sci. Rev.*, *78*, 169–187, doi:10.1016/j.quascirev.2013.08.006.

Roda-Boluda, D. C., and A. C. Whittaker (2017), Structural and geomorphological constraints on active normal faulting and landscape evolution in Calabria, Italy, *J. Geol. Soc. London.*, jgs2016-097, doi:10.1144/jgs2016-097.

Rohling, E. J., G. L. Foster, K. M. Grant, G. Marino, A. P. Roberts, M. E. Tamisiea, and F. Williams (2014), Sea-level and deep-sea-temperature variability over the past 5.3 million years, *Nature*, *508*(7497), 477–482, doi:10.1038/nature13230.

Saillard, M., S. R. Hall, L. Audin, D. L. Farber, V. Regard, and G. Hérail (2011), Andean coastal uplift and active tectonics in southern Peru: 10Be surface exposure dating of differentially uplifted marine terrace sequences (San Juan de Marcona, ~15.4°S), *Geomorphology*, *128*(3–4), 178–190, doi:10.1016/j.geomorph.2011.01.004.

Scarfì, L., G. Barberi, C. Musumeci, and D. Patanè (2016a), Seismotectonics of northeastern Sicily and southern Calabria (Italy): New constraints on the tectonic structures featuring in a crucial sector for the central Mediterranean geodynamics, *Tectonics*, *35*(3), 812–832, doi:10.1002/2015TC004022.

Scarfì, L., G. Barberi, C. Musumeci, and D. Patanè (2016b), Seismotectonics of northeastern Sicily and southern Calabria (Italy): New constraints on the tectonic structures featuring in a crucial sector for the central Mediterranean geodynamics, *Tectonics*, *35*(3), 812–830, doi:10.1002/2015TC004022.

Scicchitano, G., V. Lo Presti, C. R. Spampinato, M. Gasparo Morticelli, F. Antonioli, R. Auriemma, L. Ferranti, and C. Monaco (2011), Millstones as indicators of relative sea-level changes in northern Sicily and southern Calabria coastlines, Italy, *Quat. Int.*, *232*(1–2), 92–104, doi:10.1016/j.quaint.2010.08.019.

Selvaggi, G., and C. Chiarabba (1995), Seismicity and P-wave velocity image of the Southern
Tyrrhenian subduction zone, *Geophys. J. Int.*, *121*(3), 818–826, doi:10.1111/j.1365-
246X.1995.tb06441.x.

Serpelloni, E., M. Anzidei, P. Baldi, G. Casula, and A. Galvani (2005), Crustal velocity and strain-
rate fields in Italy and surrounding regions: new results from the analysis of permanent and non-
permanent GPS networks, *Geophys. J. Int.*, *161*(3), 861–880, doi:10.1111/j.1365-
246X.2005.02618.x.

Serpelloni, E., G. Vannucci, S. Pondrelli, A. Argnani, G. Casula, M. Anzidei, P. Baldi, and P.
Gasperini (2007), Kinematics of the Western Africa-Eurasia plate boundary from focal
mechanisms and GPS data, *Geophys. J. Int.*, *169*(3), 1180–1200, doi:10.1111/j.1365-
246X.2007.03367.x.

Serpelloni, E., C. Faccenna, G. Spada, D. Dong, and S. D. P. Williams (2013), Vertical GPS ground
motion rates in the Euro-Mediterranean region: New evidence of velocity gradients at different
spatial scales along the Nubia-Eurasia plate boundary, *J. Geophys. Res. Solid Earth*, *118*(11),
6003–6024, doi:10.1002/2013JB010102.

Siddall, M., E. J. Rohling, A. Almogi-Labin, C. Hemleben, D. Meischner, I. Schmelzer, and D. A.
Smeed (2003), Sea-level fluctuations during the last glacial cycle, *Nature*, *423*(6942), 853–858,
doi:10.1038/nature01690.

Spampinato, C. R., G. Scicchitano, L. Ferranti, and C. Monaco (2012), Raised Holocene paleo-
shorelines along the Capo Schisò coast, Taormina: New evidence of recent co-seismic
deformation in northeastern Sicily (Italy), *J. Geodyn.*, *55*, 18–31, doi:10.1016/j.jog.2011.11.007.

Stewart, I. S., A. Cundy, S. Kershaw, and C. Firth (1997), Holocene coastal uplift in the taormina
area, northeastern sicily: Implications for the southern prolongation of the calabrian seismogenic
belt, *J. Geodyn.*, *24*(1–4), 37–50, doi:10.1016/S0264-3707(97)00012-4.

Stucchi, M. et al. (2013), The SHARE European Earthquake Catalogue (SHEEC) 1000–1899, *J.
Seismol.*, *17*(2), 523–544, doi:10.1007/s10950-012-9335-2.

Sulli, A., V. Lo Presti, M. Gasparo Morticelli, and F. Antonioli (2013), Vertical movements in NE
Sicily and its offshore: Outcome of tectonic uplift during the last 125 ky, *Quat. Int.*, *288*, 168–

182, doi:10.1016/j.quaint.2012.01.021.

Tarquini, S., I. Isola, M. Favalli, F. Mazzarini, M. Bisson, M. T. Pareschi, and E. Boschi (2007), TINITALY/01: A new Triangular Irregular Network of Italy, *Ann. Geophys.*, *50*(3), 407–425.

Tarquini, S., S. Vinci, M. Favalli, F. Doumaz, A. Fornaciai, and L. Nannipieri (2012), Release of a 10-m-resolution DEM for the Italian territory: Comparison with global-coverage DEMs and anaglyph-mode exploration via the web, *Comput. Geosci.*, *38*(1), 168–170, doi:10.1016/j.cageo.2011.04.018.

Tortorici, G., M. Bianca, G. De Guidi, C. Monaco, and L. Tortorici (2003), Fault activity and marine terracing in the Capo Vaticano area (southern Calabria) during the Middle-Late Quaternary, *Quat. Int.*, *101–102*(1), 269–278, doi:10.1016/S1040-6182(02)00107-6.

Tortorici, L., C. Monaco, C. Tansi, and O. Cocina (1995), Recent and active tectonics in the Calabrian arc (Southern Italy), *Tectonophysics*, *243*(1–2), 37–55, doi:10.1016/0040-1951(94)00190-K.

Trincardi, F., and N. Zitellini (1987), The rifting of the Tyrrhenian Basin, *Geo-Marine Lett.*, *7*(1), 1–6, doi:10.1007/BF02310459.

Vacchi, M., A. Rovere, N. Zouros, S. Desruelles, V. Caron, and M. Firpo (2012), Spatial distribution of sea-level markers on Lesvos Island (NE Aegean Sea): Evidence of differential relative sea-level changes and the neotectonic implications, *Geomorphology*, *159–160*, 50–62, doi:10.1016/j.geomorph.2012.03.004.

Valensise, G., and D. Pantosti (1992), A 125 Kyr-long geological record of seismic source repeatability: the Messina Straits (southern Italy) and the 1908 earthquake (M s 7/ 2), *Terra Nov.*, *4*(4), 472–483, doi:10.1111/j.1365-3121.1992.tb00583.x.

Walters, R. J., J. R. Elliott, N. D'Agostino, P. C. England, I. Hunstad, J. A. Jackson, B. Parsons, R. J. Phillips, and G. Roberts (2009), The 2009 L'Aquila earthquake (central Italy): A source mechanism and implications for seismic hazard, *Geophys. Res. Lett.*, *36*(17), L17312, doi:10.1029/2009GL039337.

Ward, S. N. (1998), On the consistency of earthquake moment release and space geodetic strain rates: Europe, *Geophys. J. Int.*, *135*, 1011–1018, doi:10.1046/j.1365-246X.1998.00658.x.

Wells, D. L., and K. J. Coppersmith (1994), New empirical relationships among magnitude, rupture

length, rupture width, rupture area, and surface displacement, *Bull. Seismol. Soc. Am.*, *84*(4), 974–1002.

Westaway, R. (1993), Quaternary uplift of southern Italy, *J. Geophys. Res.*, *98*(B12), 741–772, doi:10.1029/93JB01566.

Wortel, M. J., and W. Spakman (2000), Subduction and slab detachment in the Mediterranean-Carpathian region., *Science*, *290*(5498), 1910–1917, doi:10.1126/science.290.5498.1910.

Yeats, R. (2012), *Active Faults of the World*, Cambridge University Press, Cambridge.

Yeats, R. S., and C. S. Prentice (1996), Introduction to Special Section: Paleoseismology, *J. Geophys. Res. Solid Earth*, *101*(B3), 5847–5853, doi:10.1029/95JB03134.

Table 1 – Previous dating of palaeoshorelines lying within the investigated area by *Scicchitano et al.* [2011], *Giunta et al.* [2012] and *Sulli et al.* [2013]. Note that different dating methods have confirmed the age (125 ky) of a prominent marine terrace along the strike of fault and over its tip. Details about their location are shown in Figure 2a and b.

Reference	Dating Method	Dated sample description	Profile number	Reported Age (ky)	Assigned Highstand (ka)	Palaeo-shoreline Elevation (m a.s.l)
Scicchitano et al., 2011 and Sulli et al., 2013	U/Th dating	*"A shell of Spondylus sp collected within thick marine deposit constituted by coarse polygenic conglomerates, micro-conglomerates and crossed lamination sands."*	6	100 - 125	125	53
Giunta et al., 2012	OSL dating	*"Yellow shore sands from unconsolidated marine sands."*	10	118 ± 7	125	61
Giunta et al., 2012	OSL dating	*"Sandy levels from unconsolidated marine sands."*	14/15	283 ± 22	285	208

Table 2 - We show all mapped inner edges from DEM and fieldwork with age assigned via synchronous correlation. This table also shows different ages sequentially-assigned by *Giunta et al.* [2012] leading them to derive fluctuating uplift rate values through time. Note that we were unable to check all locations of inner edges mapped through DEM analysis in the field because the investigated area is thickly-vegetated and densely-populated with private properties**.**

Palaeoshoreline (Profile number)	DEMs Elevations (m)	Expected Elevations (m)	Field Elevations (m)	Giunta's Elevations (m)	Our proposed Age (kyrs)	Age proposed by Giunta et al., 2012 (kyrs)	UTM Coordinate
3 (1)	57	59	-	57	125	125	33 S 0475871 4219672
7 (1)	99	99	-	99	240	200	33 S 0476308 4219436
3 (2)	57	59	-	57	125	125	33 S 0474722 4217578
7 (2)	98	98	-	98	240	200	33 S 0475083 4217269
3 (3)	54	54	-	54	125	125	33 S 0474353 4217219
7 (3)	87	89	-	87	240	200	33 S 0474511 4216876
3 (4)	49	50	-	49	125	125	33 S 0473994 4216902
7 (4)	80	79	-	-	240	-	33 S 0474049 4216761
10 (4)	124	124	-	124	340	200	33 S 0474265 4216425
3 (5)	51	51	50	51	125	125	33 S 0473639 4216783
7 (5)	81	84	85	-	240	-	33 S 0473912 4216612
9 (5)	98	93	-	98	310	200	33 S 0473868 4216424
10 (5)	125	131	120	-	340	-	33 S 0473996 4216277
3 (6)	53	53	50	53	125	125	33 S 0472871 4216042
7 (6)	83	86	85	-	240	-	33 S 0473005 4215984
9 (6)	100	96	110	100	310	200	33 S 0473260 4215861

3 (7)	54	51	-	54	125	125	33 S 0472915 4215755
10 (7)	129	131	-	129	340	200	33 S 0473105 4215415
3 (8)	56	56	-	56	125	125	33 S 0472539 4215404
7 (8)	96	93	-	96	240	200	33 S 0472701 4215060
3 (9)	55	54	54	55	125	125	33 S 0471586 4215093
7 (9)	88	89	75	88	240	200	33 S 0471462 4214794
9 (9)	102	99	100	-	310	-	33 S 0471767 4214611
3 (10)	61	63	-	61	125	125	33 S 0470269 4213855
7 (10)	105	105	115	105	240	200	33 S 0470442 4213664
9 (10)	123	121	-	-	310	-	33 S 0470528 4213527
10 (10)	152	161	145	-	340	-	33 S 0470823 4213768
1 (11)	26	21	-	-	76	-	33 S 0469214 4213892
2 (11)	50	42	-	50	100	76	33 S 0469289 4213580
3 (11)	87	89	-	87	125	125	33 S 0469370 4213279
5 (11)	125	129	-	125	200	200	33 S 0469435 4213057
7 (11)	150	156	-	-	240	-	33 S 0469528 4212622
9 (11)	190	186	-	-	310	-	33 S 0469673 4212322
10 (11)	230	233	-	-	340	-	33 S 0469861 4212020
11 (11)	274	270	-	-	410?	-	33 S 0470076 4211665
1 (12)	25	28	-	25	76	76 (?)	33 S 0468440 4213543
2 (12)	50	51	-	50	100	76 (?)	33 S 0468458 4213177
3 (12)	100	100	-	100	125	125	33 S 0468478 4212907
6 (12)	143	147	-	-	200	-	33 S 0468480 4212536
7 (12)	180	177	-	180	240	200	33 S 0468453 4212205

10 (12)	264	263	-	264	340	340	33 S 0468424 4211752
2 (13)	52	57	-	52	100	76	33 S 0467832 4213228
3 (13)	105	108	-	105	125	125	33 S 0467886 4212584
6 (13)	149	159	-	140 (?)	200	200 (?)	33 S 0467996 4212239
7 (13)	200	192	-	-	240	-	33 S 0468052 4211966
9 (13)	228	232	-	-	310	-	33 S 0468046 4211866
10 (13)	291	284	278	300	340	340	33 S 0467955 4211523
1 (14)	27	33	-	40	76	76 (?)	33 S 0467030 4213264
2 (14)	64	57	-	64	100	76 (?)	33 S 0467078 4212875
3 (14)	109	108	-	109	125	125	33 S 0467227 4212394
6 (14)	155	159	-	146 (?)	200	200 (?)	33 S 0467206 4212147
7 (14)	187	192	-	-	240	-	33 S 0467153 4211987
8 (14)	208	204	-	208	285	285	33 S 0467140 4211866
10 (14)	288	284	-	288	340	340	33 S 0467020 4211313
1 (15)	40	38	-	40	76	76 (?)	33 S 0466553 4213014
2 (15)	61	64	-	61	100	76 (?)	33 S 0466577 4212733
3 (15)	112	116	-	112	125	125	33 S 0466629 4212216
5 (15)	174	173	-	174	200	200	33 S 0466644 4211888
8 (15)	225	224	-	225	285	285	33 S 0466664 4211696
9 (15)	253	254	-	253	310	340	33 S 0466677 4211574

Table 3 - Values of sea-level highstands derived from *Siddall et al.* [2003] used to calculate predicted palaeoshoreline elevations given a value for uplift rate.

Age (ka)	Elevation of highstands (mm)
0	0
30	-80000
50	-60000
76	-30000
100	-25000
125	5000
175	-30000
200	-5000
217	-30000
240	-5000
285	-30000
310	-22000
340	5000
410	-5000
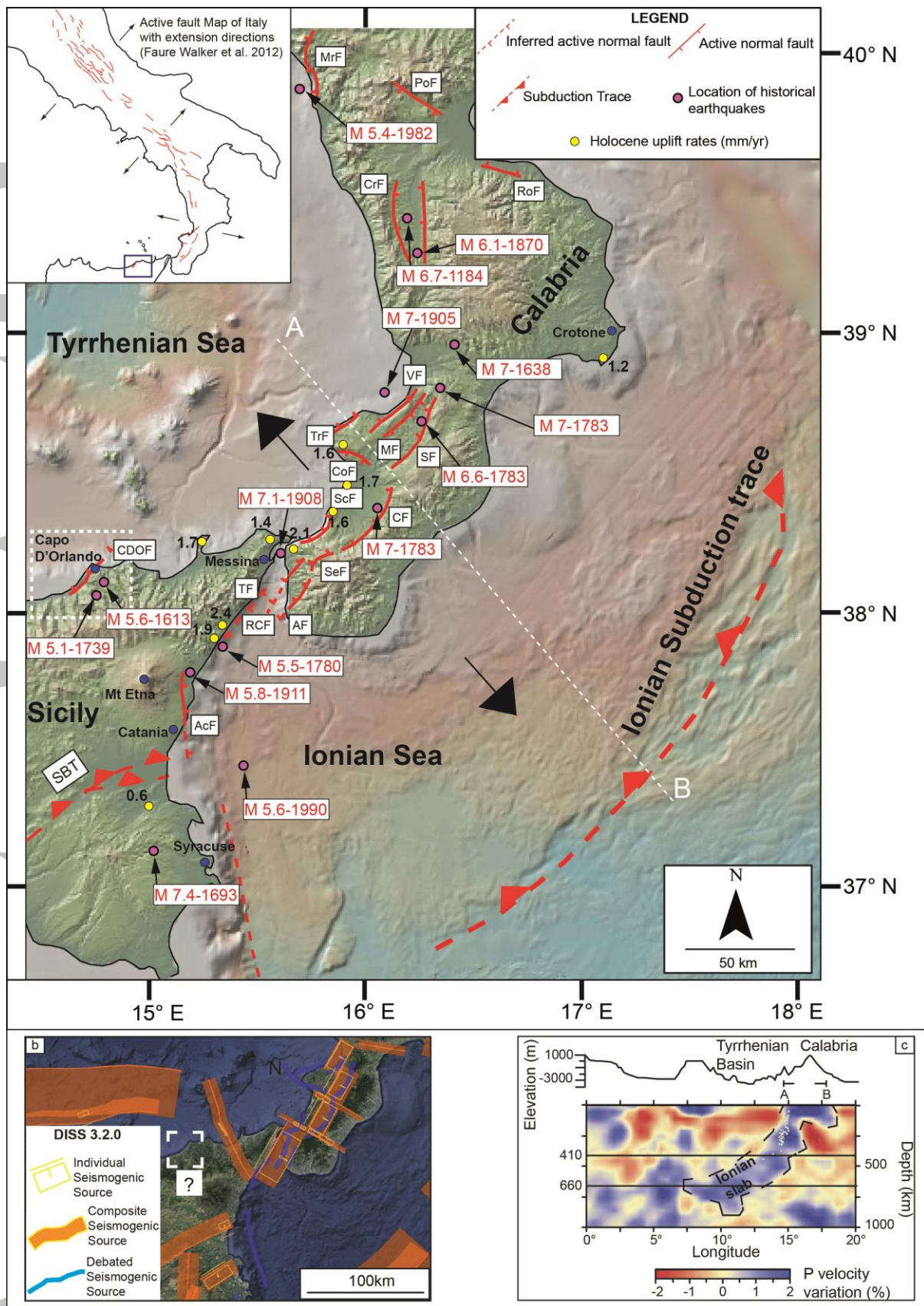
Figure. 1. Location map showing the tectonic setting of Calabria and NE Sicily. Pink dots represent

locations for historical earthquakes with the associated earthquake magnitude from *Guidoboni et al.*

[2007]. Yellow dots show Holocene uplift rate values by *Antonioli et al.*, [2006, 2009]. White-coloured dashed square shows the investigated area. Reported active normal faults are from *Michetti et al.*, [1997], *Monaco and Tortorici*, [2000], *Bianca et al.* [2011], *Giunta et al.* [2012] and *Roberts et al.*, [2013]: MrF: Maratea Fault, PoF: Pollino Fault, CrF: Crati Fault, RoF: Rossano Fault VF: Vibo Fault, TrF: Tropea Fault, CoF: Coccorino Fault, MF: Mileto Fault, SeF: Serre Fault, CF: Cittanova Fault, SeF: Sant'Eufemia Fault, ScF: Scilla Fault, AF: Armo Fault, RCF: Reggio Calabria Fault, TF: Taormina Fault, AcF: Acireale Fault, CDOF: Capo D'Orlando Fault, SBT: Sicilian Basal Thrust. Note that the CDF (Capo D'Orlando Fault) has not been reported within DISS as shown in inset b. In inset c amended tomographic cross-section from the Gulf of Lion to the Calabrian Arc by [*Lucente et al.*, 2006] is shown. Section trace A-B shows the Ionian slab beneath the Calabrian Arc characterized by intermediate and deep earthquakes (white dots).
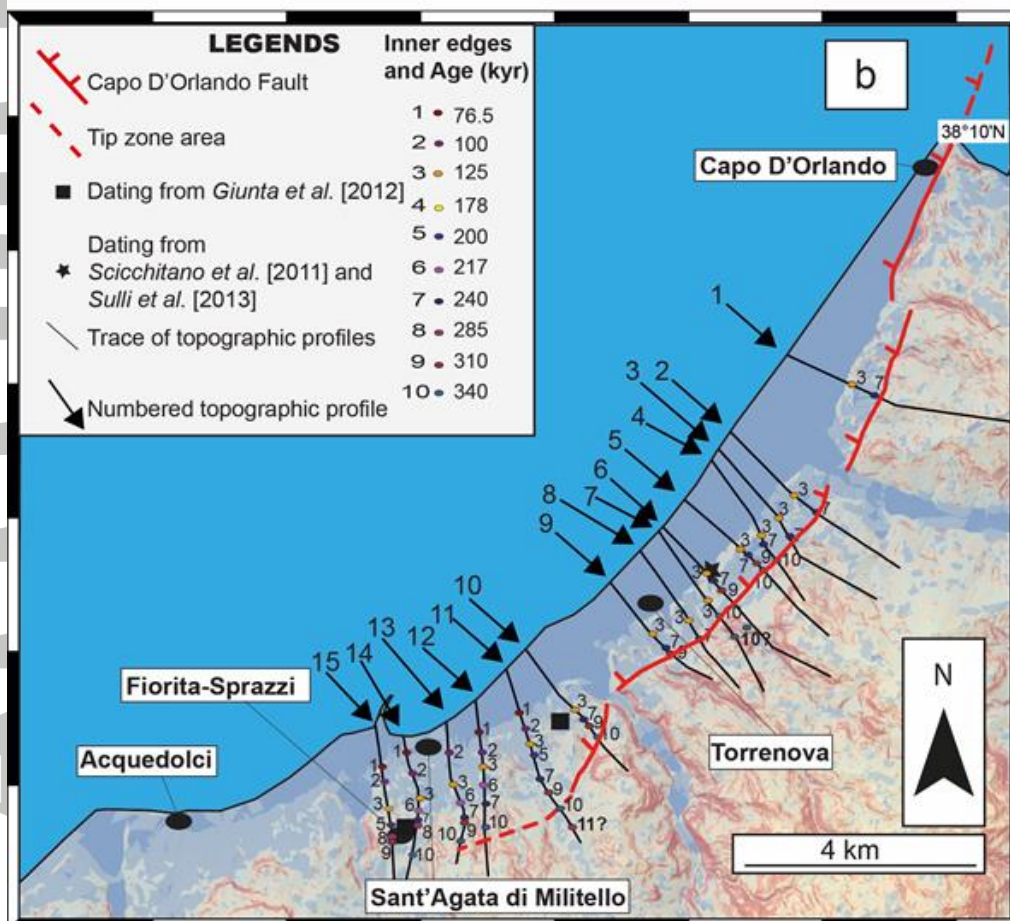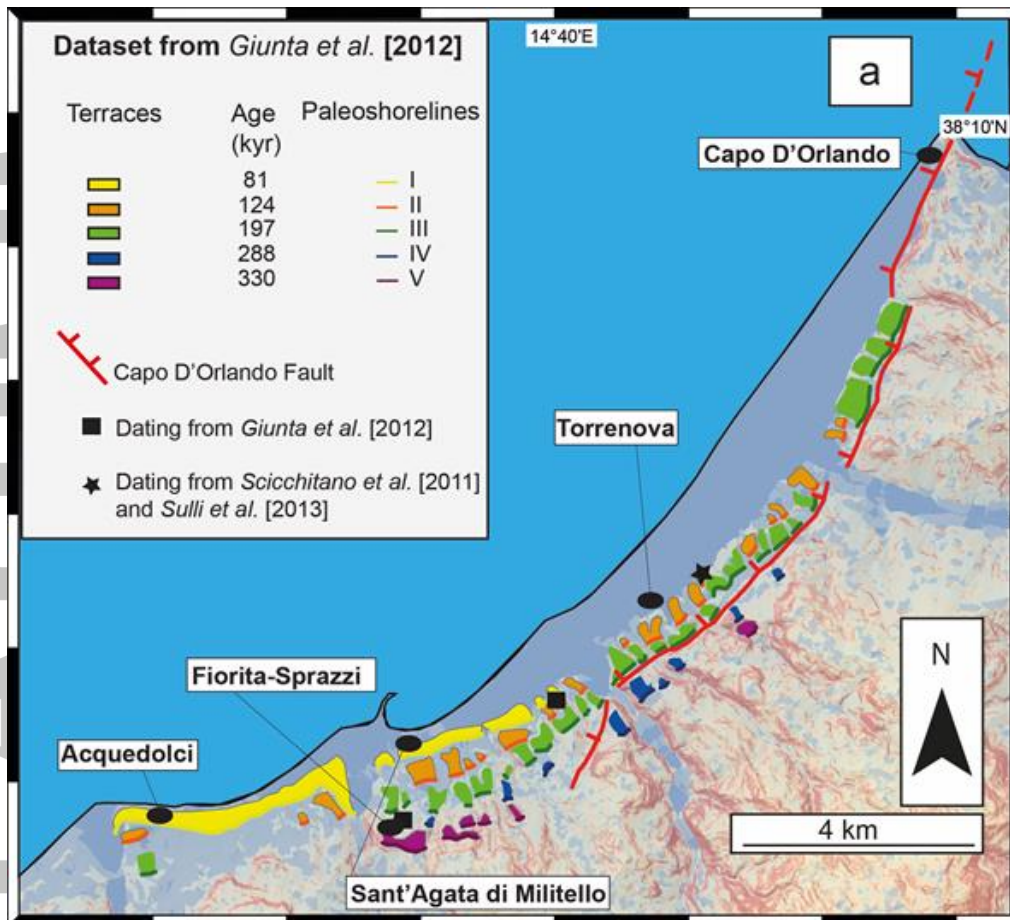
Figure 2. Location maps for palaeoshorelines within the hangingwall of the Capo d'Orlando active normal fault. A 10-m resolution DEMs with the associated coloured Slope to highlight breaking-slopes is used as base-map. In (a) is shown amended map from *Giunta et al.* [2012] showing the investigated area from Capo d'Orlando town to Santa Agata di Militello town. Location and ages of marine terraces from *Giunta et al.* [2012] are shown as well as locations of U/Th dating and OSL dating by *Scicchitano et al.* [2011] and *Giunta et al.* [2012]. In (b) inner edges of marine terraces with our reviewed ages (see numbered dots and the associated age within Legends panel), the "tip zone" area marked in the SW with red-coloured dashed line and 15-topographic profile locations are shown from this study.
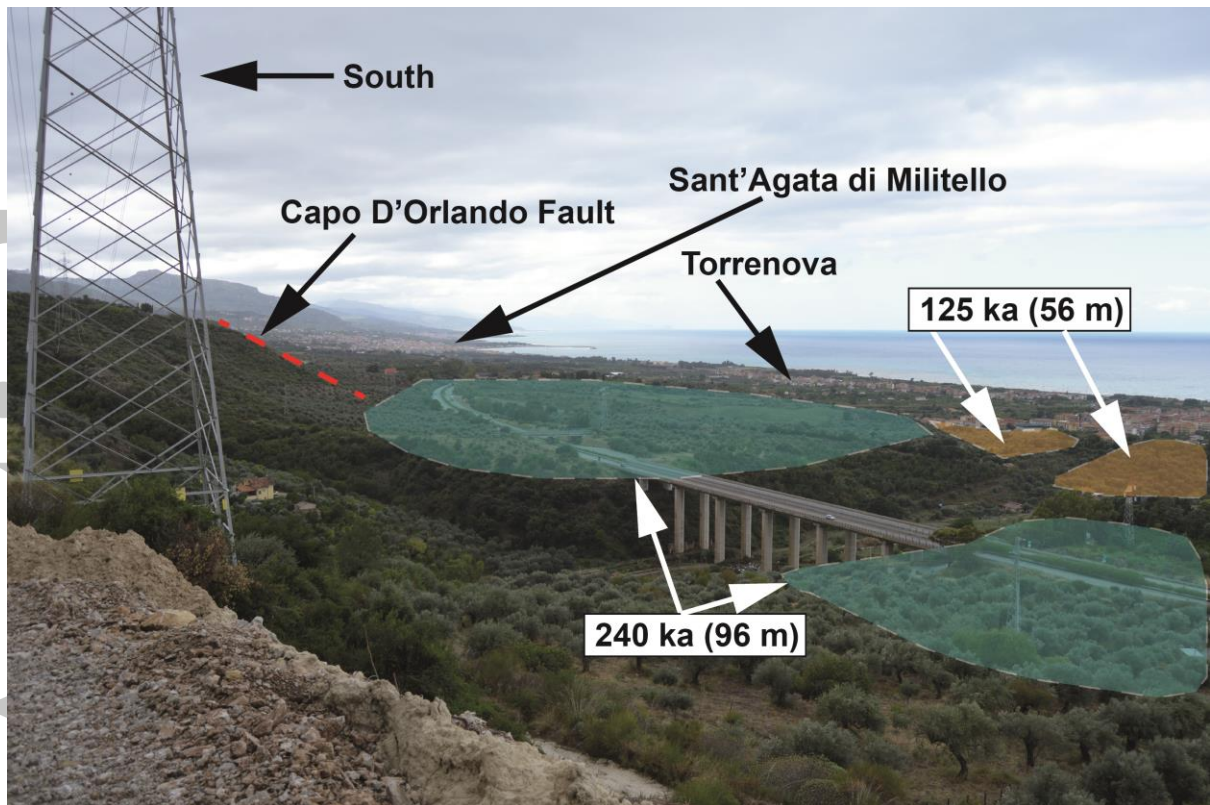
Figure 3. View of interpreted marine terraces in the field (shaded polygons) within the Profile 8 with the associated inner edge elevations and the synchronously-assigned ages. The synchronous correlation approach allowed us to reassign the age of 240 ky to the palaeoshoreline at 96 m previously [*Giunta et al.*, 2012] sequentially-assigned to the 200 ka sea-level highstand.
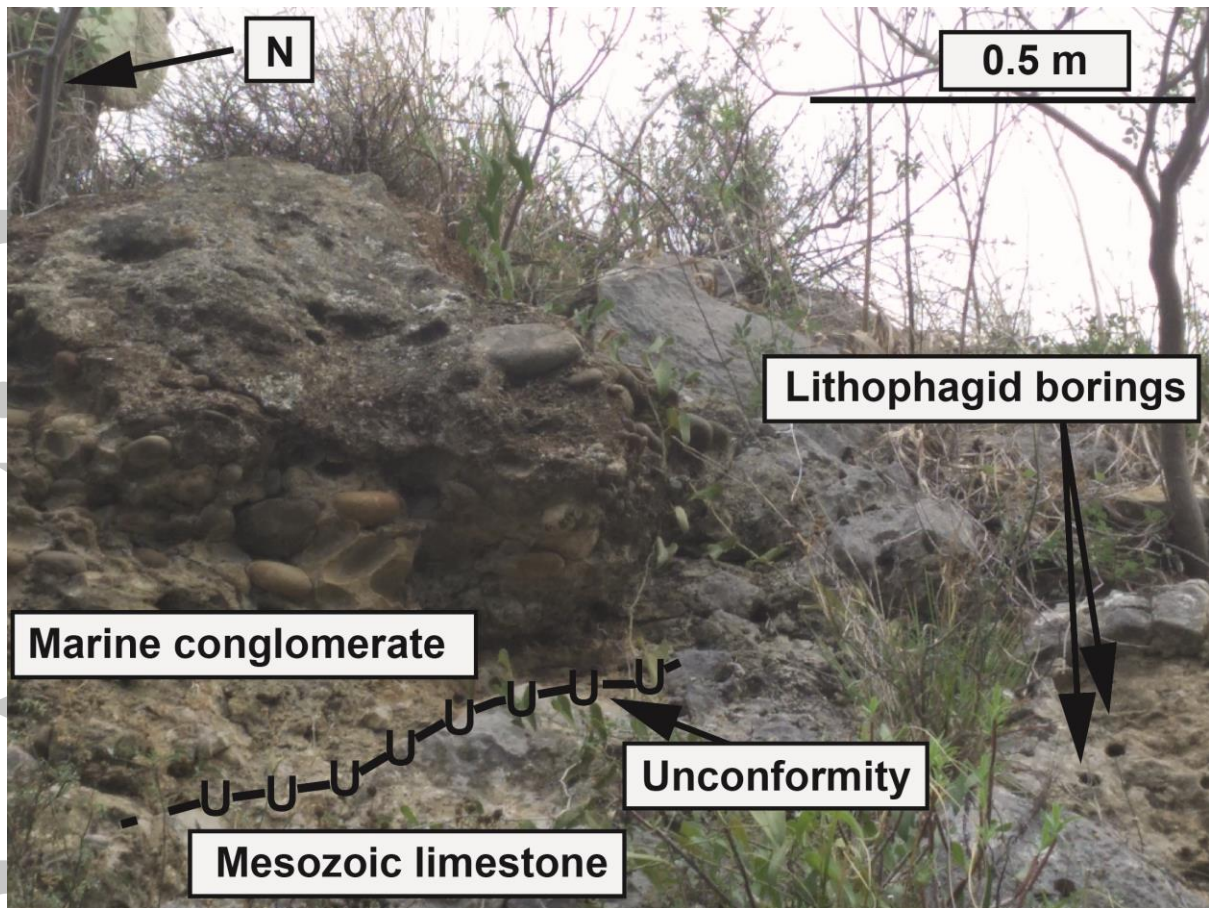
Figure 4. Field evidence, lying along Profile 6, of inner edge showing upper palaeoshoreface depositional environment. The picture shows a marine abrasion platform made of Mesozoic limestone unconformably overlain by marine conglomeratic deposits already well-described by *Scicchitano et al.* [2011] and *Giunta et al.* [2012]. In places lithophagid borings into Mesozoic limestone and scattered evidence of beach cobbles have been mapped close this area, suggesting the presence of the 125ka-dated palaeoshoreline. This inner edge could have not been mapped in the DEMs due to the resolution.
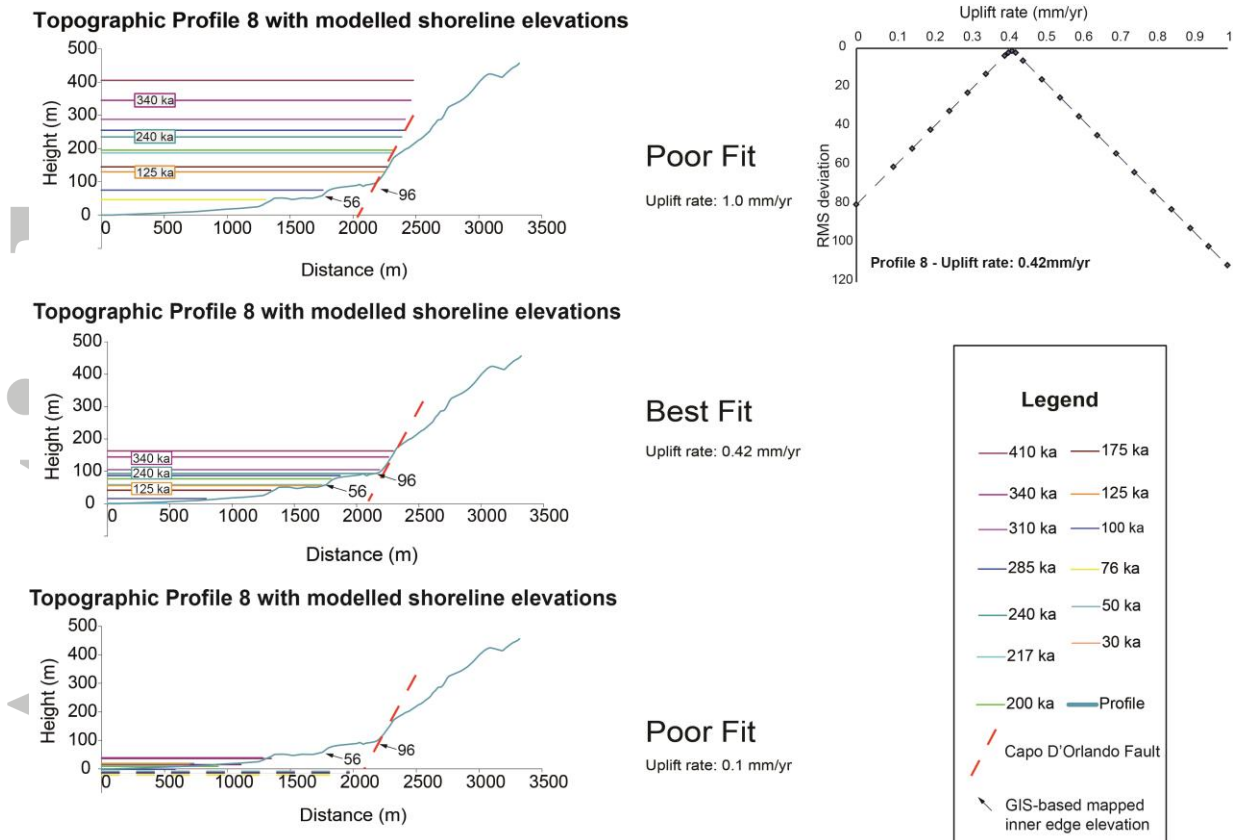
Figure 5. Example of a modelled topographic profile (profile 8 herein) showing a synchronously-modelled sequence of marine terraces on the hangingwall of the Capo D'Orlando Fault by iterating uplift rates values to find the best match between mapped palaeoshorelines (using GIS analysis and/or fieldwork) and the predicted sea-level highstands (coloured lines). RMS devation vs Uplift rates (mm/yr) is shown, suggesting that our preferred uplift rate is very robust. Note that our "best fit" is based on the fact that the iteration of uplift rate values is driven by a dated horizon/palaeoshoreline (125 ka). RMS deviation calculations for each topographic profile are shown in the Supplementary material.

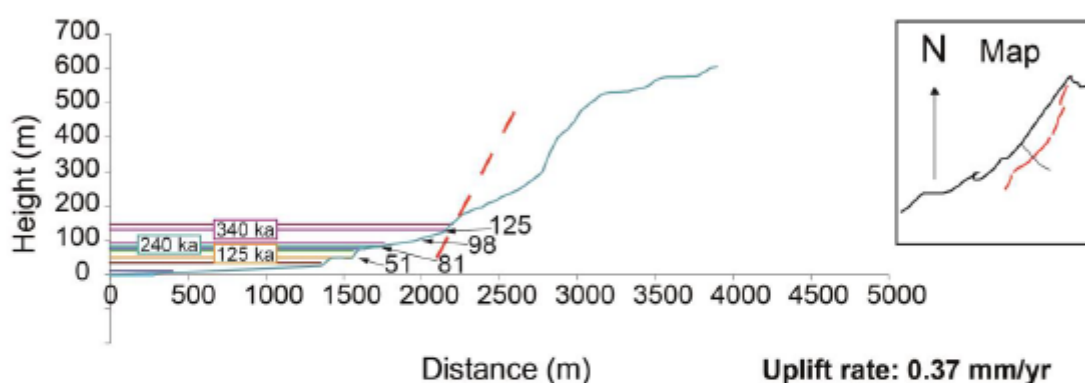Topographic Profile 1 with modelled shoreline elevations

Uplift rate: 0.43 mm/yr
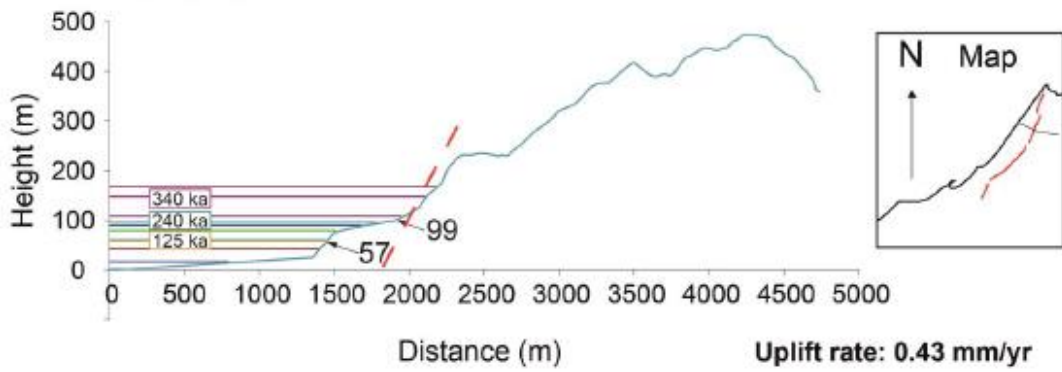
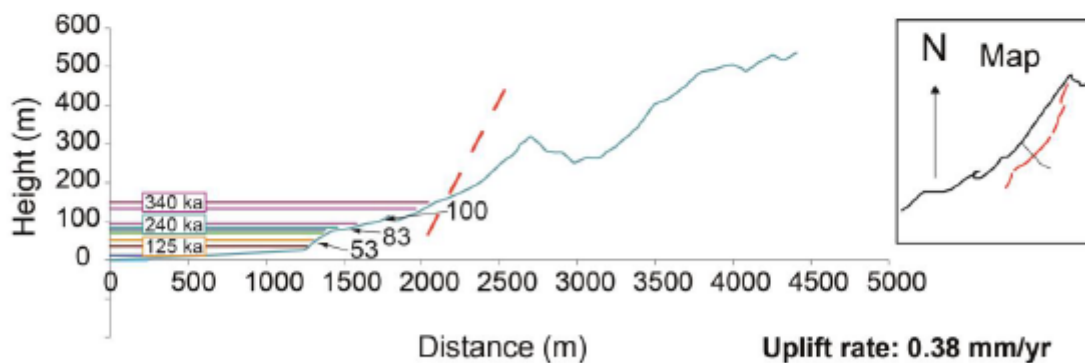Topographic Profile 2 with modelled shoreline elevations

Uplift rate: 0.43 mm/yr
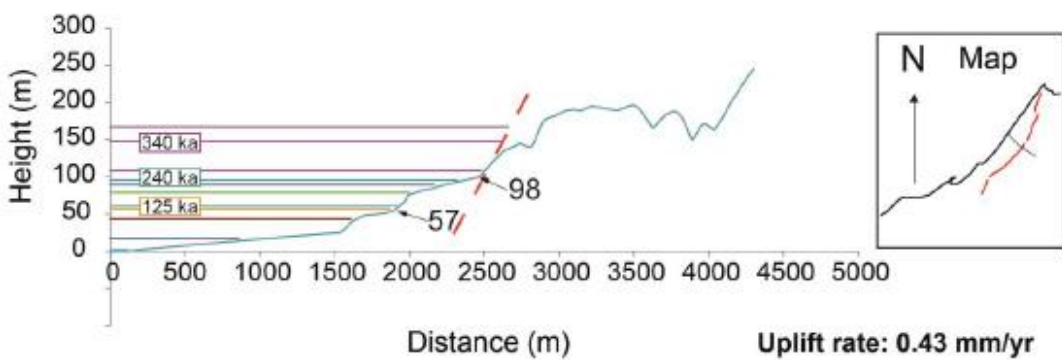
Topographic Profile 3 with modelled shoreline elevations

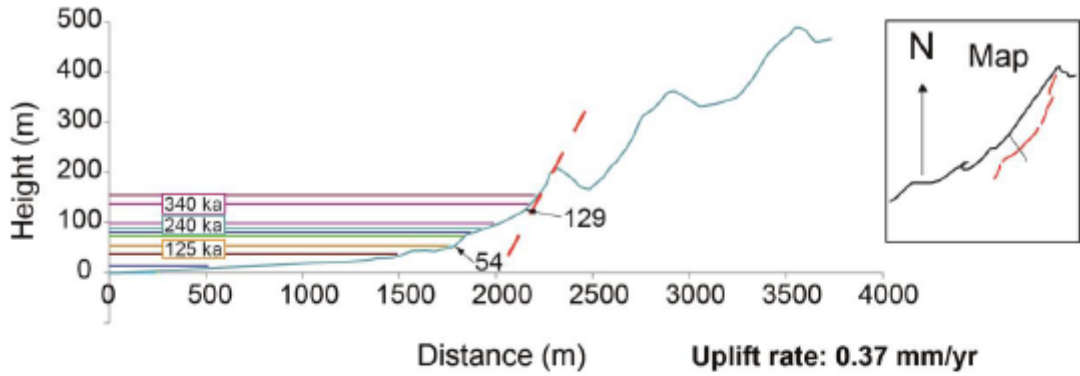Uplift rate: 0.39 mm/yr

Legend:
GIS-based mapped inner edge elevation   Capo D'Orlando Fault
410 ka — 310 ka — 240 ka — 200 ka — 125 ka — 76 ka — 30 ka
340 ka — 285 ka — 217 ka — 175 ka — 100 ka — 50 ka — Profile
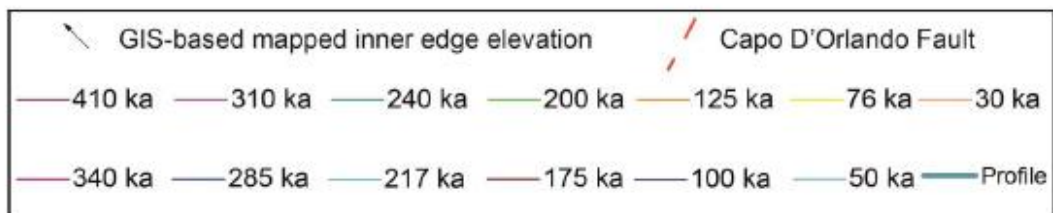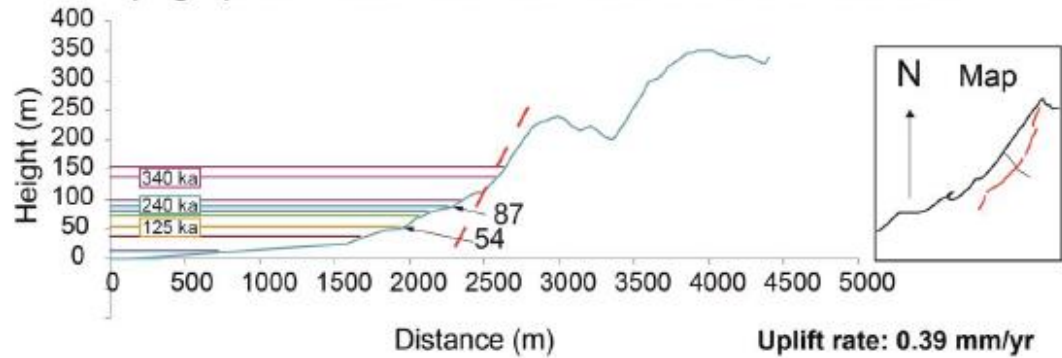
Topographic Profile 4 with modelled shoreline elevations

Uplift rate: 0.35 mm/yr
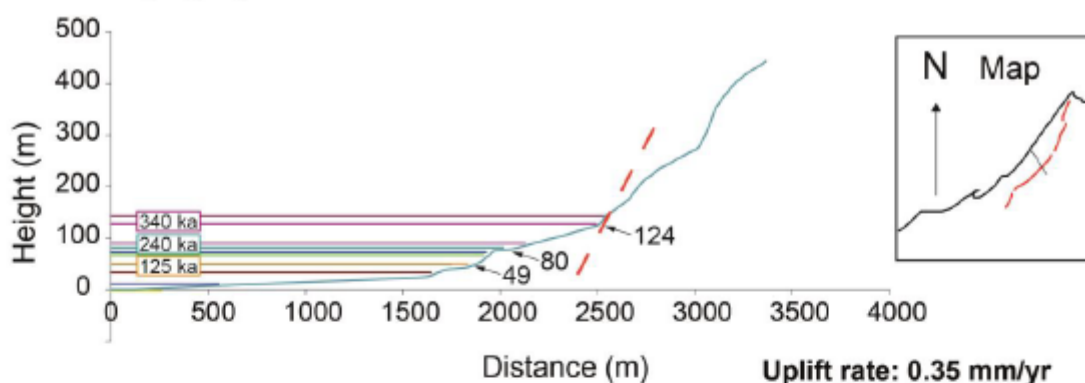
Topographic Profile 5 with modelled shoreline elevations

Uplift rate: 0.37 mm/yr

Topographic Profile 6 with modelled shoreline elevations

Uplift rate: 0.38 mm/yr

Legend:
- GIS-based mapped inner edge elevation
- Capo D'Orlando Fault
- 410 ka — 310 ka — 240 ka — 200 ka — 125 ka — 76 ka — 30 ka
- 340 ka — 285 ka — 217 ka — 175 ka — 100 ka — 50 ka — Profile
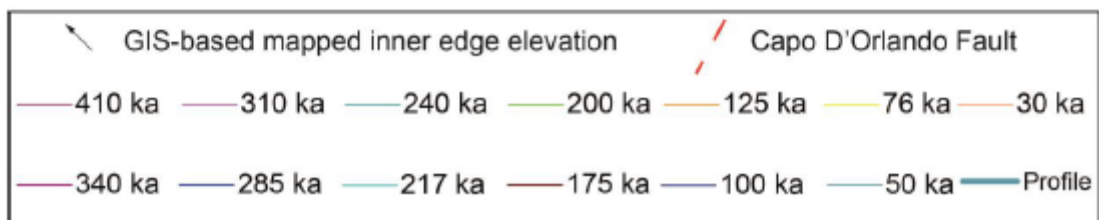
Topographic Profile 7 with modelled shoreline elevations

340 ka
240 ka
125 ka
129
54

Distance (m)　　Uplift rate: 0.37 mm/yr

Topographic Profile 8 with modelled shoreline elevations

340 ka
240 ka
125 ka
56
96

Distance (m)　　Uplift rate: 0.41 mm/yr
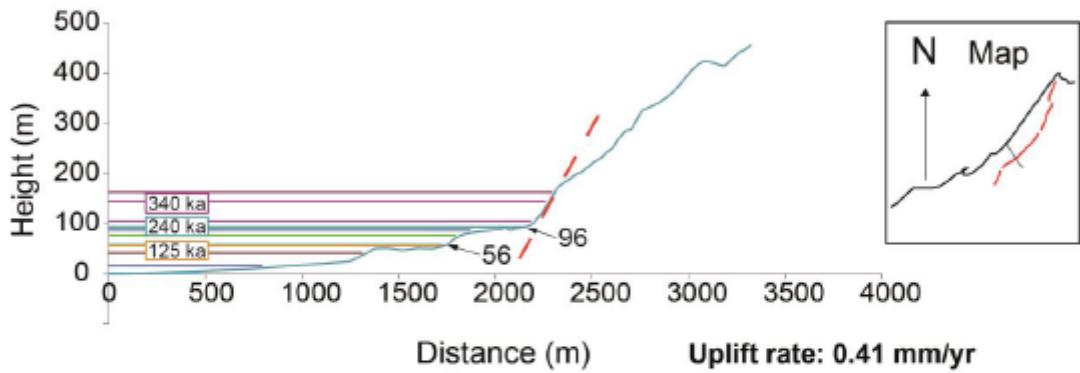
Topographic Profile 9 with modelled shoreline elevations

340 ka
240 ka
125 ka
102
88
55

Distance (m)　　Uplift rate: 0.39 mm/yr

GIS-based mapped inner edge elevation　　Capo D'Orlando Fault

410 ka	310 ka	240 ka	200 ka	125 ka	76 ka	30 ka
340 ka	285 ka	217 ka	175 ka	100 ka	50 ka	Profile
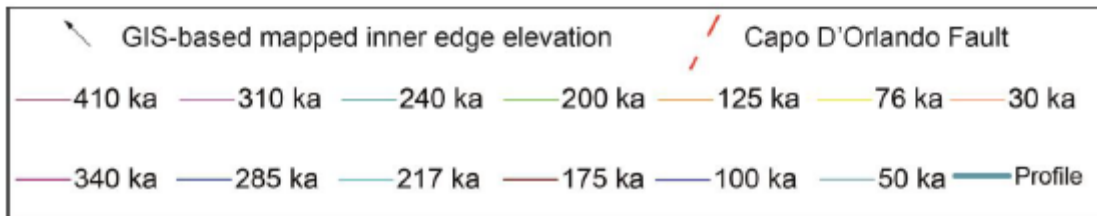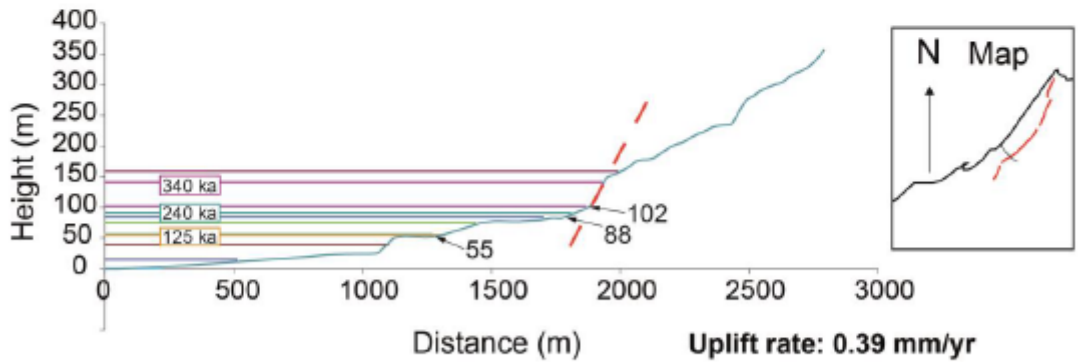
Topographic Profile 10 with modelled shoreline elevations

Height (m) vs Distance (m)

340 ka, 240 ka, 125 ka

152, 123, 105, 61

Uplift rate: 0.46 mm/yr
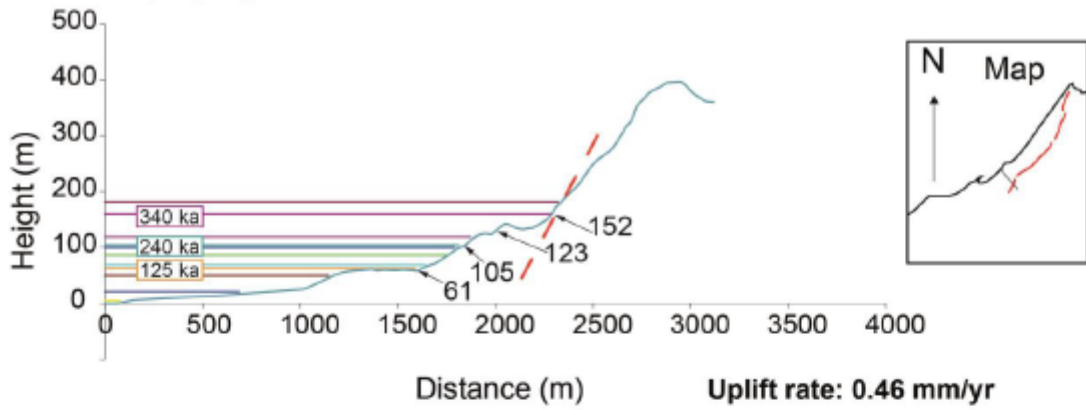
Topographic Profile 11 with modelled shoreline elevations

Height (m) vs Distance (m)

340 ka, 240 ka, 125 ka

274?, 230, 190, 150, 125, 87, 50, 26

Uplift rate: 0.67 mm/yr
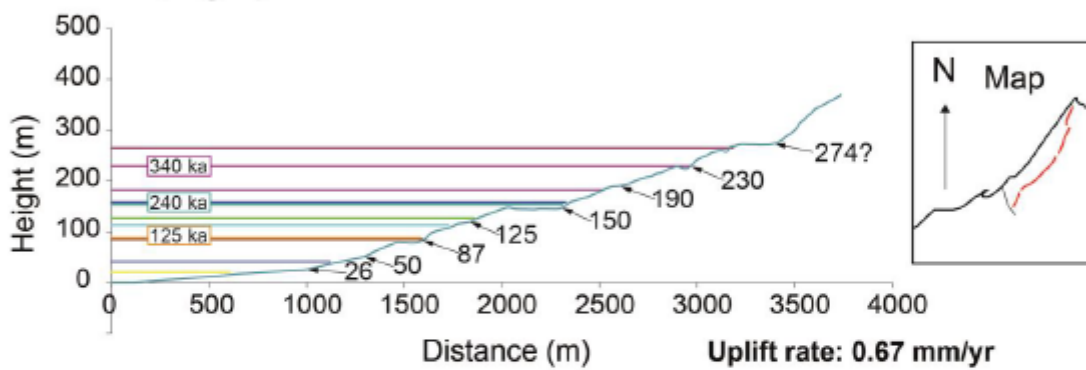
Topographic Profile 12 with modelled shoreline elevations

Height (m) vs Distance (m)

340 ka, 240 ka, 125 ka

264, 180, 143, 100, 50, 25

Uplift rate: 0.76 mm/yr

Legend:

GIS-based mapped inner edge elevation — Capo D'Orlando Fault

— 410 ka — 310 ka — 240 ka — 200 ka — 125 ka — 76 ka — 30 ka

— 340 ka — 285 ka — 217 ka — 175 ka — 100 ka — 50 ka — Profile

Topographic Profile 13 with modelled shoreline elevations

Height (m)

340 ka
291
240 ka
228
200
125 ka
149
105
52

Distance (m)   Uplift rate: 0.82 mm/yr

N   Map

Topographic Profile 14 with modelled shoreline elevations

Height (m)

340 ka
288
240 ka
208
187
125 ka
155
109
64
27

Distance (m)   Uplift rate: 0.82 mm/yr

N   Map

Topographic Profile 15 with modelled shoreline elevations

Height (m)

253
240 ka
225
174
125 ka
112
61
40

Distance (m)   Uplift rate: 0.89 mm/yr

| GIS-based mapped inner edge elevation | Capo D'Orlando Fault |

— 410 ka — 310 ka — 240 ka — 200 ka — 125 ka — 76 ka — 30 ka

— 340 ka — 285 ka — 217 ka — 175 ka — 100 ka — 50 ka — Profile

Figure 6. Topographic profiles derived by using 10-m high-resolution Digital Elevation Models [*Tarquini et al.*, 2007, 2012] showing modelled and mapped palaeoshoreline elevations. The coloured lines represent the sea-level highstands (or predicted palaeoshoreline elevations) calculated by iterating

uplift rate values to find the best match with the mapped (numbered arrows) palaeoshorelines. More

detailed profiles locations on Figure 2b. Inner edge elevations with refined ages are also shown in Table
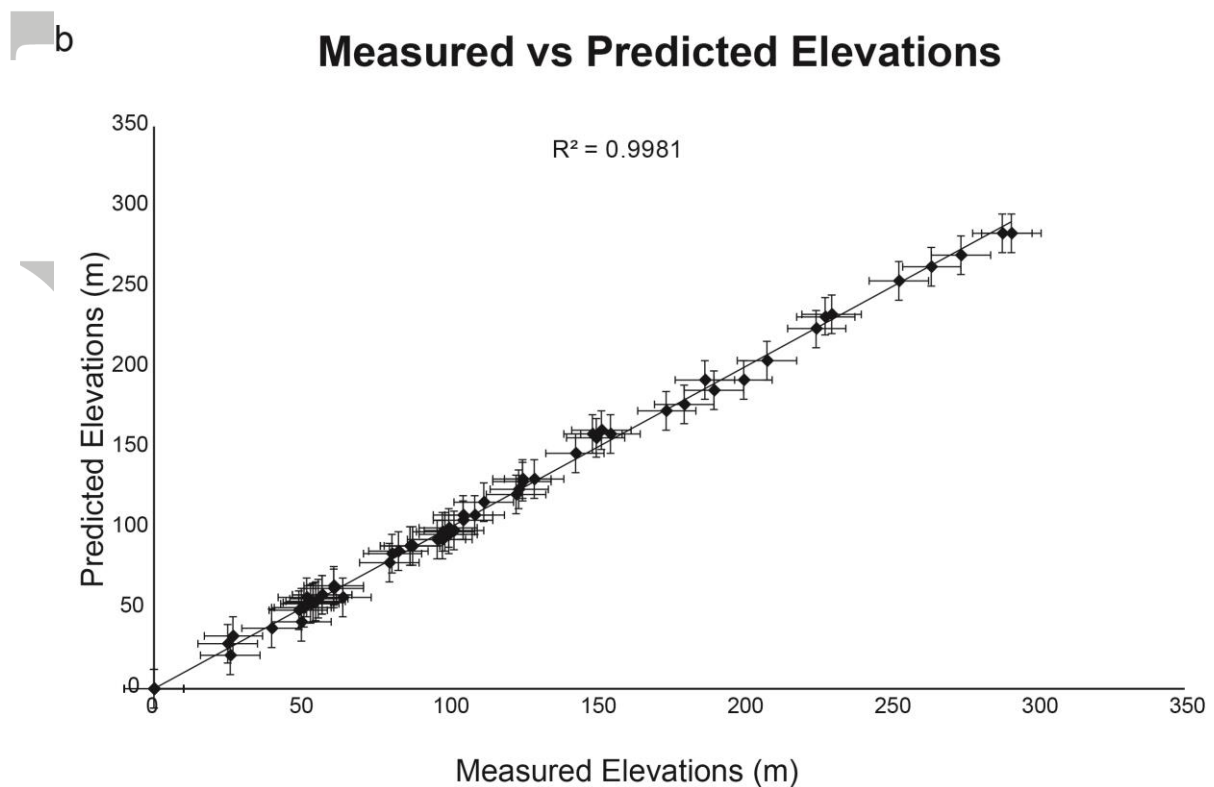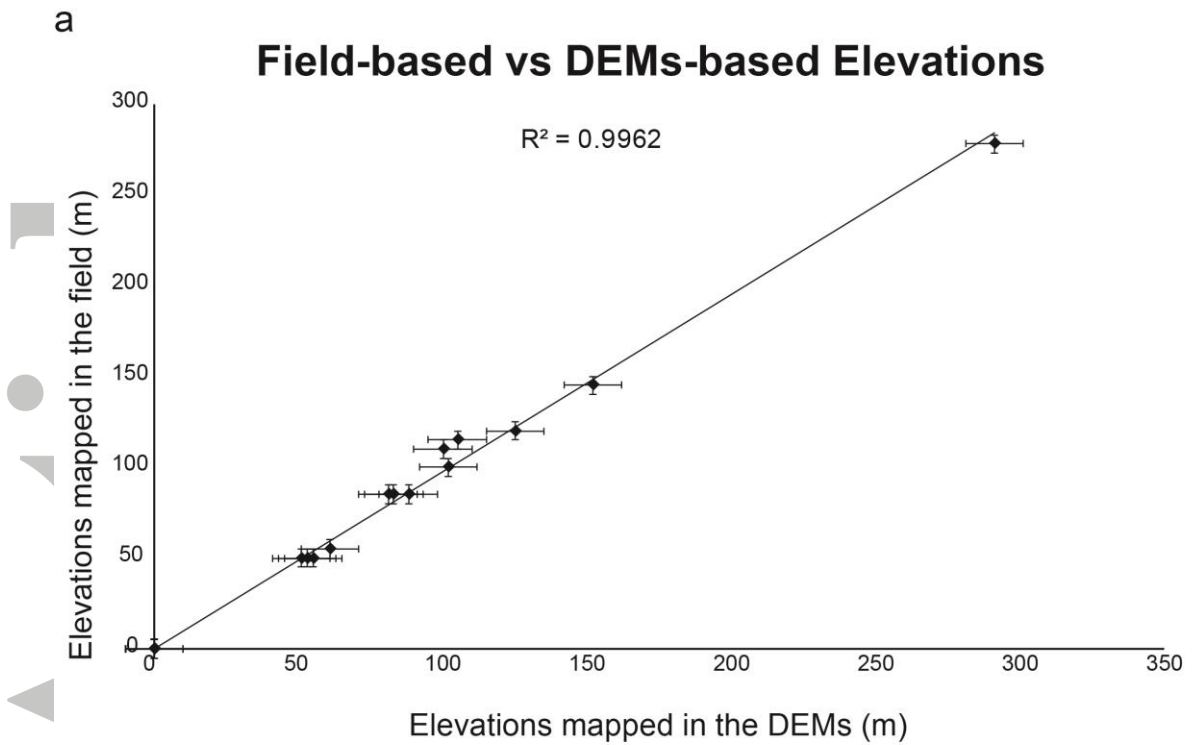
2

Figure 7. In (a) the graph is showing the relationship between field-based and DEM-based inner edge elevations. The R^2 value > 0.99 confirms a very robust relationship suggesting that elevations measured elsewhere in the DEM are likely to be accurate. In (b) the graph is showing linear regression analysis

between our measured and predicted elevations. The predicted elevations, representing the synchronously-calculated sea-level highstand elevations, have been derived by defining a constant uplift rate through time, and iterating this value to find the best match to the measured and mapped palaeoshorelines.
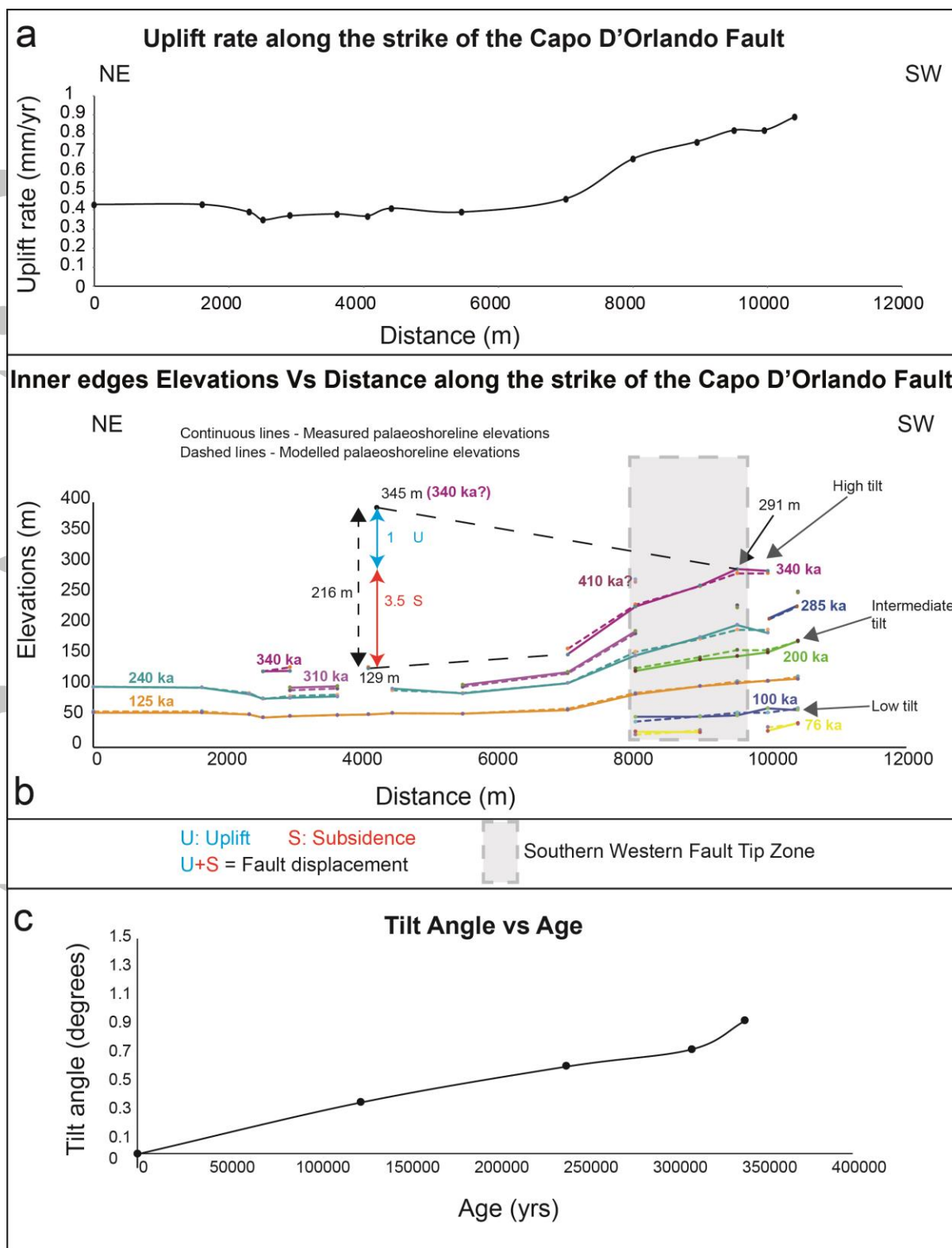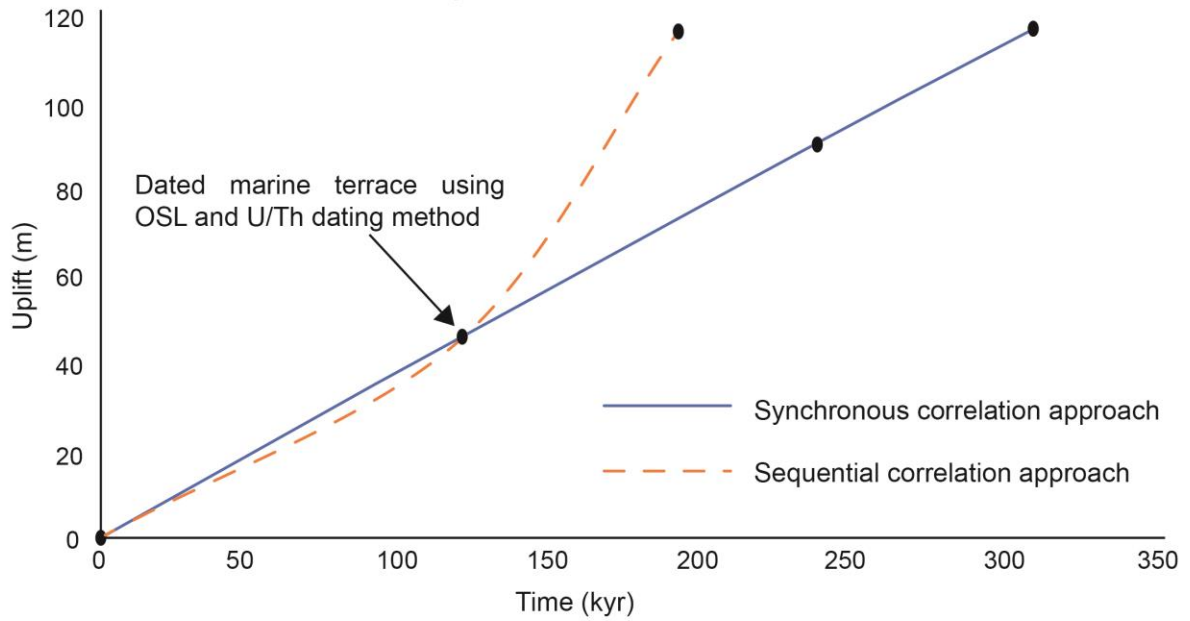
Figure 8. Diagrams showing evidence of Quaternary Capo D'Orlando Fault activity. In (a) uplift rates is spatially varying along strike the Capo D'Orlando Fault. In (b) palaeoshoreline elevations are changing along the strike of the Capo D'Orlando Fault. Solid lines represent our mapped and measured palaeoshoreline elevations mapped by using DEMs and checked in the field; closely-dashed coloured

lines represent modelled iteratively-calculated sea-level highstand elevations (or the expected elevations) mostly matching with the solid lines. Uplift/Subsidence ratio (U:S) value of 1/3.5 has been applied to the oldest (340 ka) palaeoshoreline mapped within the hangingwall to estimate the expected elevation on the footwall and derive long-term fault slip-rate. A black dashed arrowed line shows the displacement between terraces mapped in the hangingwall and footwall cut-offs. In (c) the faulting activity of Capo D'Orlando Fault over the Late Quaternary has tilted the investigated marine terraces; in fact, older and higher palaeoshorelines show higher tilt angle values because they have been experiencing a longer history of faulting activity.
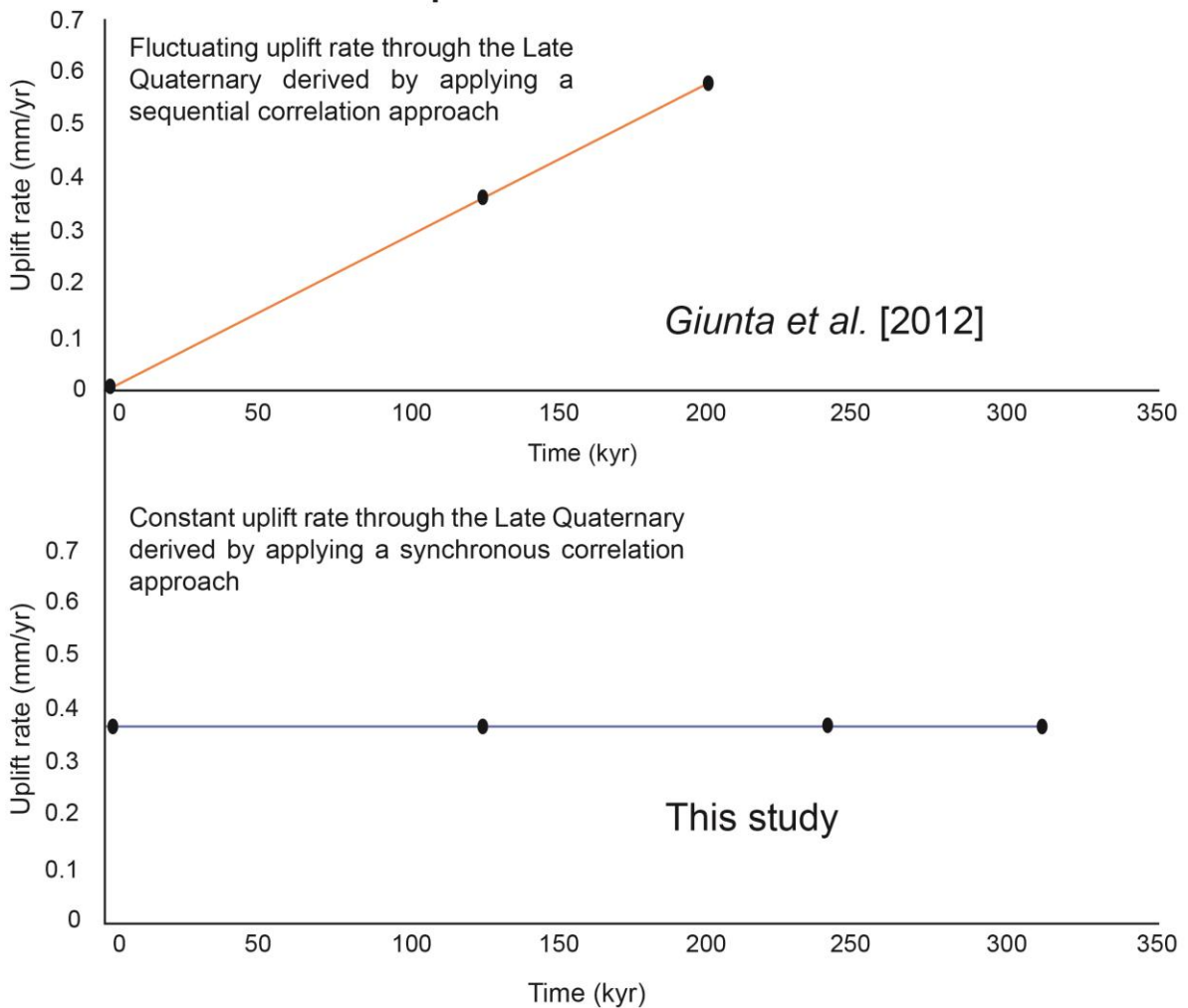
a Uplift vs Time

Dated marine terrace using OSL and U/Th dating method

— Synchronous correlation approach

--- Sequential correlation approach

b Uplift rate vs Time

Fluctuating uplift rate through the Late Quaternary derived by applying a sequential correlation approach

Giunta et al. [2012]

Constant uplift rate through the Late Quaternary derived by applying a synchronous correlation approach

This study

Figure 9. In (a) uplift gradients are shown derived from [*Giunta et al.,* 2012] (orange-coloured dashline) and this study (blue line). The orange-coloured dash line shows an exponential growth of the uplift gradient through time driven by an absolutely-dated palaeoshoreline (125 ka). Instead, the blue-coloured line shows a constant growth of the uplift gradient through time also driven by an absolutely-dated palaeshoreline (125 ka). Note that changing uplift rates through time is also shown in Figure 7 (section 2) in *Giunta et al.,* [2012].
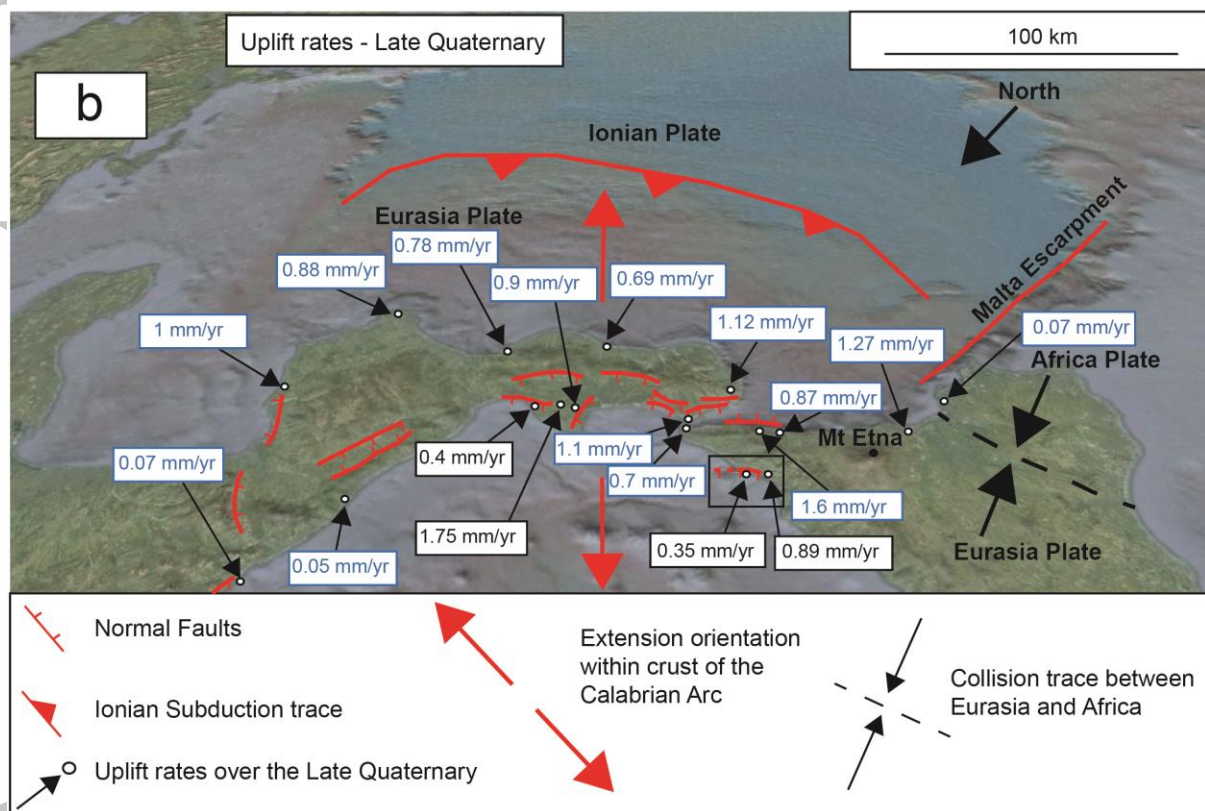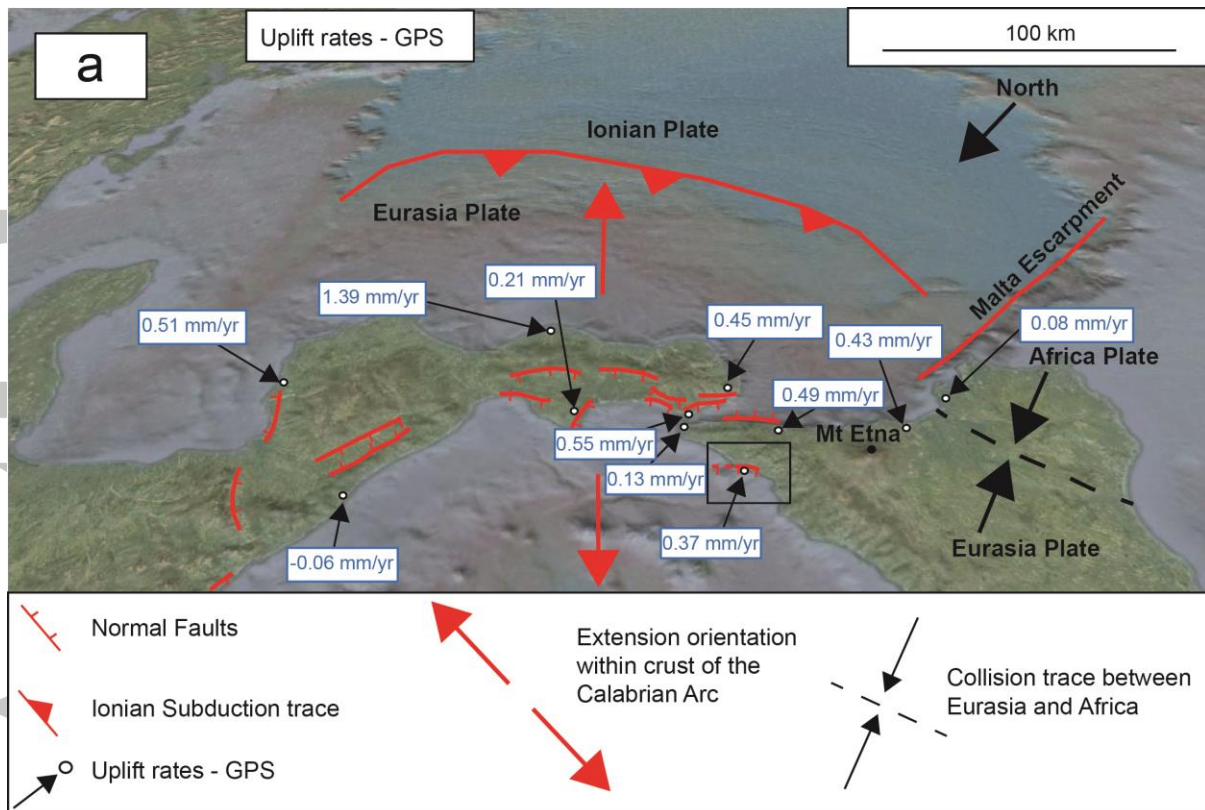
Figure 10. Regional extension accommodated by normal faults within the upper plate of the Ionian

Subduction Zone, along the geological domain of Calabrian Arc, is shown. In (a) prominent changing

uplift rates from GPS analysis (light blue values) [*Serpelloni et al.*, 2013] are shown along the Calabrian

Arc. Similarly, in (b) Late Quaternary uplift rates change by up to a factor of 4 across the Calabrian

Arc, with large variations between the footwalls and hangingwall of faults, and along the strike of faults

towards fault tips, suggesting prominent heterogeneity for slip on subduction interface through time.

Light blue values in b are reported by *Catalano and De Guidi*, [2003] and *Ferranti et al.* [2006], and

black values are reported from this study (black square) and *Roberts et al.* [2013].